Canard-like explosion of limit cycles in two-dimensional piecewise-linear models of FitzHugh-Nagumo type

.

NJIT CAMS Technical Report
1112-4

Horacio G. Rotstein [1]*, Stephen Coombes [2], Ana Maria Gheorghe [2],

[1] Department of Mathematical Sciences
New Jersey Institute of Technology
Newark, NJ 07102, USA
[2] School of Mathematical Sciences
University of Nottingham
Nottingham NG7 2RD, UK

Abstract

We investigate the mechanism of abrupt transition between small and large amplitude oscillations in fast-slow piecewise-linear (PWL) models of FitzHugh-Nagumo (FHN) type. In the context of neuroscience, these oscillatory regimes correspond to subthreshold oscillations and action potentials (spikes) respectively. The minimal model that shows such phenomenon has a cubic-like nullcline (for the fast equation) with two or more linear pieces in the middle branch and one piece in the left and right branches. Simpler models with only one linear piece in the middle branch or a discontinuity between the left and right branches (McKean model) show a single oscillatory mode. As the number of linear pieces increases, PWL models of FHN type approach smooth FHN-type models. For the minimal model, we investigate the bifurcation structure, we describe the mechanism that leads to the abrupt, canard-like transition between subthreshold oscillations and spikes, and we provide an

*Also, Center for Applied Mathematics and Statistics, New Jersey Institute of Technology. E-mail: horacio@njit.edu

analytical way of predicting the amplitude regime of a given limit cycle trajectory which includes the approximation of the canard critical control parameter. We extend our results to models with a larger number of linear pieces. Our results for PWL-FHN type models are consistent with similar results for smooth FHN type models. In addition, we develop tools that are amenable for the investigation of a variety of related, and more complex, problems including forced, stochastic and coupled oscillators.

1 Introduction

In a two-dimensional relaxation oscillator, the canard phenomenon (or canard explosion) refers to the abrupt increase in the amplitude of the limit cycle created in a Hopf bifurcation as a control parameter crosses a very small critical range which is exponentially small in the parameter defining the slow time scale [1, 2, 3, 4, 5, 6, 7]. Depending on whether the Hopf bifurcation is supercritical or subcritical, the small amplitude limit cycles are either stable or unstable respectively. The large amplitude, relaxation-type limit cycles are always stable.

We illustrate the canard phenomenon for both cases in Fig. 1 for a smooth, fast-slow system of FitzHugh-Nagumo (FHN) type of the form

$$\begin{cases} v' = f(v) - w, \\ w' = \epsilon\, [\, \alpha\, v - \lambda - w\,], \end{cases} \tag{1}$$

where α, λ and ϵ are constants, $0 < \epsilon \ll 1$, $\alpha > 0$, and $f(v)$ is a cubic-like function. We used $\epsilon = 0.01$ and the prototypical cubic function $f(v) = -h\, v^3 + a\, v^2$ with $h = 2$ and $a = 3$ whose maximum and minimum occur at $(0, 0)$ and $(1, 1)$ respectively. This canonical choice ensures that the large amplitude oscillations are $\mathcal{O}(1)$. The parameters α and λ control the slope of the w-nullcline $N_w = \alpha\, v - \lambda$ and its position relative to the v-nullcline $N_v = f(v)$ respectively. In the context of neuroscience, the variables v and w correspond to a dimensionless voltage and a recovery variable respectively, and the parameter λ can be thought of as a dimensionless externally applied (DC) current, after redefining $w \to w + \lambda$. In Appendix A we provide a technical discussion about the Hopf bifurcation and canard phenomenon for these systems.

For $\lambda = 0$ the v- and w-nullclines in Fig. 1 (N_v and N_w respectively) intersect at the minimum of the cubic nullcline N_v. For the parameters we used, the Hopf bifurcation is supercritical (subcritical) for $\alpha > 3$ ($\alpha < 3$) (see Appendix A). Consequently, the Hopf bifurcation is supercritical in Figs. 1-A ($\alpha = 4$) and subcritical in Figs. 1-B ($\alpha = 2$). The left panels show sketches of the graphs of the limit cycle amplitude versus the control parameter λ ($A = 0$ indicates a fixed point). In both cases, the Hopf bifurcation occurs as λ crosses $\lambda_H = \mathcal{O}(\epsilon) > 0$ (see Appendix A). For values of $\lambda < \lambda_H$ ($\lambda > \lambda_H$) the fixed-points are stable (unstable). In the supercritical case (Fig. 1-A), the fixed-point is the only attractor for $\lambda < \lambda_H$ and the system is excitable [8, 9, 10, 11]. In the subcritical case (Fig. 1-B), there is bistability for a range of values of λ where large amplitude oscillations and a fixed point coexist.

The small amplitude limit cycles created at $\lambda = \lambda_H$ are stable in the supercritical case (Fig. 1-A) and unstable in the subcritical case (Fig. 1-B). Their amplitude increases slowly for values of λ close to λ_H. In the supercritical case (Fig. 1-A) this happens as λ increases. As λ crosses from

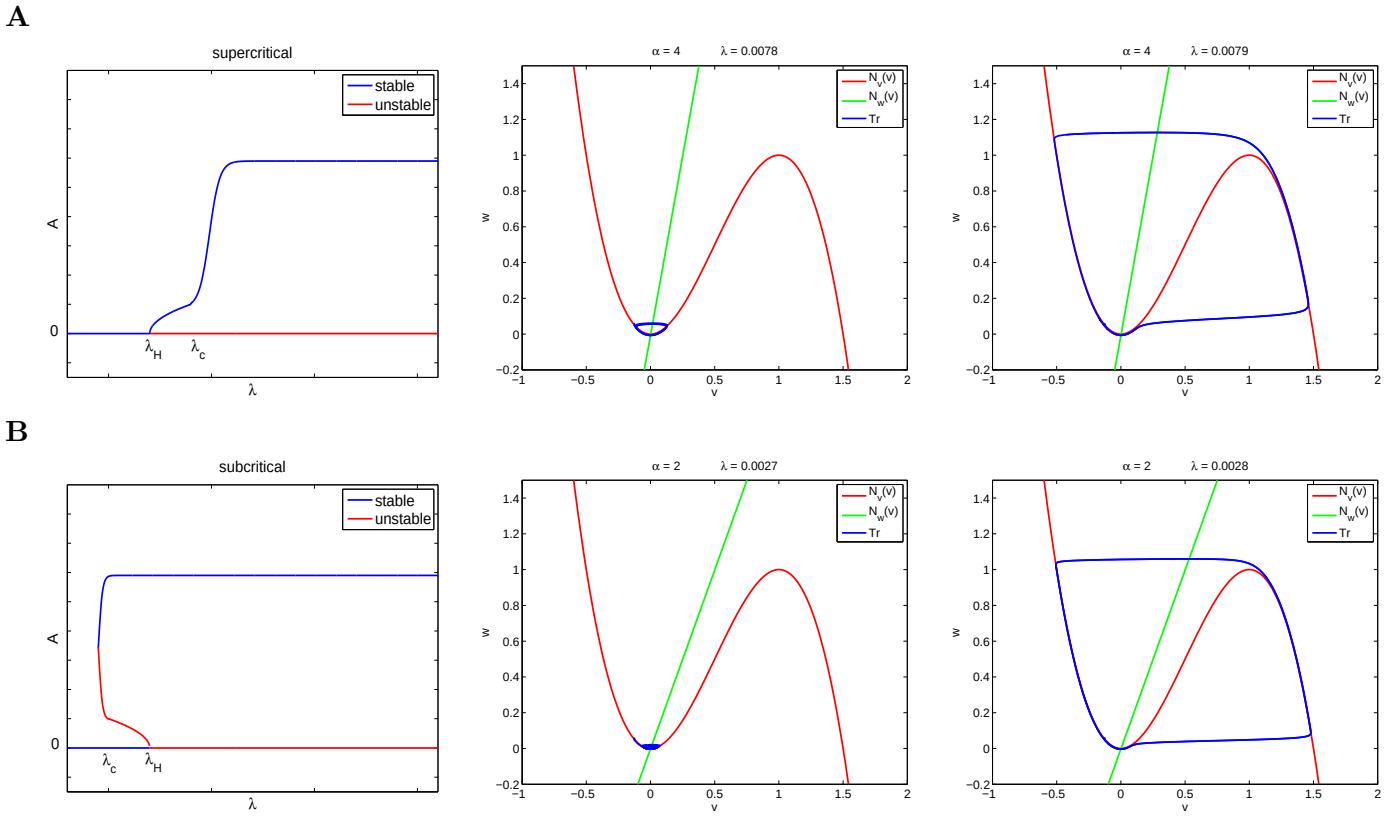

Figure 1: **Supercritial and subcritical canard phenomenon (canard explosion) for the FHN model** (1) with $f(v) = -2\,v^3 + 3\,v^2$, $\epsilon = 0.01$ and various values of α and λ. **Left panels:** bifurcation diagrams. $A = 0$ corresponds to fixed-points, $A > 0$ corresponds to the amplitude of limit cycles, λ_H and λ_c indicate the Hopf bifurcation and canard critical points respectively. **Middle and right panels:** phase-planes for representative values of λ. N_v and N_w represent the v- and w-nullclines respectively and Tr represents the trajectory. **A** Supercritical case: $\lambda_H \sim 0.0025$ and $\lambda_c \sim 0.0078$. Small amplitude limit cycles are stable. **B** Subcritical case: $\lambda_H \sim 0.0035$ and $\lambda_c \sim 0.00278$. Small amplitude limit cycles are unstable. The trajectory shown in the middle panel displays damped oscillations and converges to the stable fixed-point.

$\lambda = 0.0078$ to $\lambda = 0.0079$ (middle to right panels), the limit cycle "explodes". The small (exponentially small in ϵ) range of values of the control parameter λ over which this canard explosion occurs can be approximated by the canard critical value $\lambda_c = 0.00782$. In the subcritical case (Fig. 1-B), the unstable small amplitude limit cycle (not shown) explodes as λ decreases below $\lambda_c = 0.00278$. The values of λ_c were computed using the formulas given in Appendix A. One feature of the canard phenomenon is that trajectories evolve in close vicinities of the unstable (middle) branch of the v-nullcline for a significant amount of time before moving either to the left or to the right to generate small and large amplitude oscillations respectively (see Fig. 1-A for example).

The canard phenomenon for smooth two-dimensional systems has been investigated by various authors. It was discovered by Benoit et al. [4] for the Van der Pol (VDP) oscillator where the w-nullcline is a vertical line (see Appendix A.3). They used non-standard analysis techniques. Eckhaus [2] and Baer et al. [3] investigated the canard phenomenon using asymptotic techniques. In particular they found expressions for λ_c for VDP- and FHN-type equations. The canard phenomenon has also been studied by Dumortier and Roussarie [1] and by Krupa and Szmolyan [5, 6] for more general two-dimensional slow-fast systems. These results assumed a set of non-degeneracy conditions which in particular imply that the v-nullcline has to be locally parabolic at its minimum. For future use, we sketch some of these results in Appendix A.

The goal of this paper is to investigate the mechanism leading to the canard explosion in two-dimensional, piecewise linear (PWL) systems of the form (1) with $f(v)$ substituted by a cubic-like PWL function. PWL caricatures of nonlinear models have been fruitfully used in a number of different branches of the applied sciences ranging from biology to mechanics as a way to provide new insights into the dynamics of smooth models or as a convenient way to explicitely analyze them when a general set of mathematical techniques is not available. For example in neuroscience the McKean model [12] may be regarded as a variant of the FitzHugh-Nagumo model [13] that provides a planar model of an excitable cell in which the dynamics is broken into simpler linear pieces. This has allowed for a number of results about the existence and stability of periodic orbits and traveling waves to be obtained [14, 15, 16, 17, 18, 19] and insight into action potential generation and response to stimulation to be obtained [20]. An extension of this approach to other single neuron models, including the Morris-Lecar model, has recently been pursued by Tonnelier and Gerstner [21] and Coombes [22]. In a mechanical setting PWL modeling has helped to shed light on the motion of rocking blocks [23] and models of suspension bridges [24], and indeed impacting systems in general (see the recent book by di Bernardo et al. [25]). Many of the techniques for analysing mechanical systems have been taken over to the study of oscillatory electronic circuits and in particular the analysis of non-smooth bifurcation such as those of border-collision type [26]. In the systems biology context techniques originally developed by Filippov [27] (for ordinary differential equations with a discontinuous vector field) have been applied to gene regulatory networks with switch-like interactions (arising in the limit of a steep sigmoidal nonlinearity) [28, 29]. From a more mathematical perspective PWL systems have allowed for the analysis of limit cycles [30] and their bifurcations [31, 32] and have been shown numerically to support canard solutions [33].

The investigation of the dynamics of PWL oscillators, and in particular the abrupt transition between limit cycle amplitude regimes provides complementary information to previous studies on

analogous smooth systems. These studies have focused on the existence of the so called canard solutions (including the so called maximal canards which exist for values of the control parameter in the small transition range between small and large amplitude limit cycles) and the conditions under which canard explosions occur, and less attention has been paid to the actual evolution of trajectories for values of λ near the critical value for the abrupt transition (λ_c). Understanding this is important not only for the understanding of the dynamics of single oscillators but also for the understanding of the effects that external inputs (e.g., pulsatile, sinusoidal, noisy and synaptic-like) exert on single oscillators and the dynamics of oscillatory networks. For small enough values of ϵ, trajectories corresponding to single oscillators can be approximated over most of their period either by the stable branches of the v-nullclines, which approximate the slow manifolds, or by the horizontal fast fibers. These phases of the oscillation are typically robust to external perturbations.

By contrast, perturbations in a range of phases in which the trajectory is evolving in a close vicinity of the unstable branch of the v-nullcline can lead to disparate effects where the resulting amplitude regime (small or large) of the perturbed system is different from that of the unperturbed one. More specifically, using neuroscience terminology, spiking can be created or suppressed, or delayed / advanced by a significant amount of time with respect to the unperturbed oscillation. The canard critical value λ_c (see Appendix A) provides information on whether the limit cycle trajectory of an unperturbed oscillator crosses the unstable branch of the v-nullcline (small amplitude oscillations) or not (large amplitude oscillations). However, when the system is perturbed the relative position between nullclines changes and so do the fixed-point and the canard-critical value. For time-dependent perturbations, the effects of these changes in evolving trajectories are difficult to predict as are the resulting amplitude regimes of perturbed trajectories. In particular, the canard critical value, that becomes time-dependent, is no longer an appropriate tool for this purpose. Asymptotic techniques can be used to provide a description of trajectories for small values of ϵ. However, even for single oscillators [2, 3] their description becomes complicated and provides little intuition on their evolution. In addition, as the value of ϵ increases to intermediate values still smaller than $\mathcal{O}(1)$ these approximations become less accurate.

In Section 2, we introduce some notation on PWL systems of FHN type, where the function $f(v)$ in (1) is substituted by a cubic-like PWL function, and we overview, for future use, the solutions to the linear regimes corresponding to each one of the linear pieces in a PWL system. In Section 3, we investigate the dynamics of PWL systems having two linear pieces in the middle branch of the cubic-like function and one linear piece in the other two. We refer to them as $\text{PWL}_{1,2,1}$ systems. These are the simplest PWL models for which canard explosions occur. In linear systems with only one linear piece in the middle branch, limit cycles have a single (large) amplitude regime. We first present the bifurcation structure of $\text{PWL}_{1,2,1}$ systems. Then, we investigate the mechanism leading to the canard-like explosion of limit cycles. Although solutions for PWL systems can be computed analytically, the insight they provide into the underlying dynamics is poor. We use dynamical systems tools to explain these dynamics and answer various relevant questions about the abrupt transition between limit cycle amplitude regimes. In addition, we provide a way of calculating analytical approximations to the canard critical value λ_c and discuss the accuracy of these approximations and the dependence of λ_c on other relevant model parameters. Finally, we show that, although the amplitude of the small limit

cycle changes with the model parameters, the period is independent of λ. In Section 4, we extend our results to PWL systems having three linear pieces in the middle branch and one linear piece in the other two. We discuss the implications of our results for more general and complex models in Section 5.

2 Piecewise linear models of FitzHugh-Nagumo type

We consider the following piecewise linear (PWL) models of FitzHugh-Nagumo (FHN) type where the cubic-like smooth function $f(v)$ in system (1) is substituted by a PWL caricature $f_{pwl}(v)$:

$$\begin{cases} v' = f_{pwl}(v) - w, \\ w' = \epsilon\,[\,\alpha\, v - \lambda - w\,]. \end{cases} \tag{2}$$

We use prototypical PWL functions $f_{pwl}(v)$ with minimum $(v_{min}, w_{min}) = (0, 0)$ and maximum $(v_{max}, w_{max}) = (1, 1)$. As in the smooth case discussed above, this choice ensures that large amplitude oscillations are $\mathcal{O}(1)$. Each branch of $f_{pwl}(v)$ consists of one or more linear pieces L_j indexed by j. The v- and w-nullclines of model (2) are given by

$$N_v = f_{pwl}(v) \qquad \text{and} \qquad N_v = \alpha\, v - \lambda \tag{3}$$

respectively.

2.1 Construction of piecewise linear functions

We refer to a cubic-like PWL function having M, M_l and M_r linear pieces in the middle, left and right branches respectively as a PWL_{M_l,M,M_r} function. If the number of linear pieces in all branches of $f(v)$ is equal ($M_l = M_r = M$), then we refer to this function as PWL_M. We use an analogous terminology for the corresponding models. We illustrate this in Fig. 2 for a $\text{PWL}_{1,2,1}$ model

In the process of building the PWL function $f_{pwl}(v)$ we use the following notation:

- We partition the interval $[v_{min}, v_{max}]$ into M segments with end-points v_j, for $j = 0, \ldots, M$, where $v_0 = v_{min}$, $v_M = v_{max}$ and $v_{j-1} < v_j$.
- We call L_j ($j = 1, \ldots, M$) the linear piece that has endpoints (v_{j-1}, w_{j-1}) and (v_j, w_j).
- We call η_j, $j = 1, \ldots, M$ the slope of the linear piece L_j.
- Given the values $v_0, \ldots, v_M$ and the first $M-1$ slopes $(\eta_1, \ldots, \eta_{M-1})$ we calculate $w_j = \eta_j\ (v_j - v_{j-1}) + w_{j-1}$ for $j = 1, \ldots, M-1$. The slope of the last piece in the middle branch is given by $\eta_M = (w_M - w_{M-1})/(v_M - v_{M-1})$.
- We proceed in a similar manner with the left and right branches. In the left branch $j = -M_l - 1, \ldots, 0$ and in the right branch, $j = M, \ldots, M + M_r$. Alternatively, we use the notation $L_{l,j}$ and $L_{r,j}$ as illustrated in Fig. 2.

2.2 PWL approximations of smooth vector fields

In order to link the cubic-like PWL functions $f_{pwl}(v)$ in eq. (2) to the corresponding smooth functions $f(v)$ in eq. (1) we use $M = M_l = M_r$ and proceed as follows:

- We call $\Delta v = (v_{max} - v_{min})/M$ and $v_j = j\,\Delta v$ for $j = -M_l, \ldots, M + M_r$ with $M = M_l = M_r$.
- We call $w_j = f(v_j)$ for $j = -M_l, \ldots, M_r$.
- We call $\eta_j = (w_j - w_{j-1})/(v_j - v_{j-1})$ for $j = -M_l + 1, \ldots, M + M_r$.

As M increases, $f_{pwl}(v)$ approaches the corresponding smooth function $f(v)$. Fig. 3 illustrates the approximation of the solutions to the corresponding PWL_M systems (2) to the smooth system (1) as M increases.

In both Figs. 3-A and -B, the top-left panels show the phase-plane diagrams corresponding to the smooth vector fields for two different values of λ which are close to the canard critical point λ_c. The parameters α and ϵ are as in Fig. 1-A (supercritical case). In Fig. 3-A, $\lambda > \lambda_c$ and the smooth system exhibit large amplitude oscillations. In Fig. 3-B, $\lambda < \lambda_c$ and the smooth system exhibits small amplitude oscillations The remaining panels in both Figs. 3-A and -B correspond to the PWL approximations for a number of linear pieces that increases from the top-middle to the bottom-right panels.

As M increases, the dynamics of the PWL system approach the dynamics of the corresponding smooth systems. For $\lambda > \lambda_c$ (Fig. 3-A), the limit cycle is in the large amplitude regime for all values of M. In contrast, for $\lambda < \lambda_c$ (Fig. 3-B), the limit cycle is in the large amplitude regime for small values of M (≤ 9) and the transition to the small amplitude oscillations regime occurs for $M = 10$. We explain the corresponding mechanism in the following sections.

2.3 Dynamics of the basic linear components

In order to investigate the dynamics of a PWL system such as (2) it is convenient to consider it divided into a number of linear regimes $\mathcal{R}_j$ associated to the linear pieces L_j. A linear regime $\mathcal{R}_j$ is a strip in the phase-plane bounded by the vertical lines crossing the end-points of the linear piece L_j, $v = \hat{v}_{j-1}$ and $v = \hat{v}_j$ respectively (see Fig. 2). More specifically, a point (v, w) in phase-plane belongs to $\mathcal{R}_j$ if $\hat{v}_{j-1} \leq v \leq \hat{v}_j$ where $\hat{v}_{j-1}$ and $\hat{v}_j$ are the v-coordinates of the left and right endpoints of the linear piece L_j. Note that two regimes corresponding to linear pieces with a joint endpoint interesect at the vertical line containing this point.

The dynamics of each linear regime $\mathcal{R}_j$ are governed by a linear system of the form

$$\begin{cases} v' = \eta_j\ (v - \hat{v}_{j-1}) + \hat{w}_{j-1} - w, \\ w' = \epsilon\ [\alpha\, v - \lambda - w], \end{cases} \tag{4}$$

where $(\hat{v}_{j-1}, \hat{w}_{j-1})$ and η_j are the left end-point and slope of the corresponding linear piece L_j respectively. The initial conditions $v_{0,j}$ and $w_{0,j}$ in each regime are equal to the values of v and w at the end of the previous one. More specifically, if $\mathcal{R}_i$ is the regime prior to $\mathcal{R}_j$ (either R_{j-1} or R_{j+1}), and

the solution in $\mathcal{R}_i$ arrives at v_i (v-coordinate of the joint point between L_i and L_j) at a time t_i, then the initial conditions for system (4) corresponding to the linear regime $\mathcal{R}_j$ are $v = v_i$ and $w = w(t_i)$.

The solutions to (4) can be calculated using standard methods [34]. We present them below and illustrate them in Section 3 tied to our explanation of the canard explosion. For simplicity, we drop the indices from the endpoints $(\hat{v}, \hat{w})$, the slope η and the initial conditions (v_0, w_0). The fixed point for system (4) is given by

$$\bar{v} = \frac{\lambda - \eta\,\hat{v} + \hat{w}}{\alpha - \eta} \qquad\qquad \bar{w} = \frac{\lambda\,\eta - \alpha\,\eta\,\hat{v} + \alpha\,\hat{w}}{\alpha - \eta}. \tag{5}$$

The eigenvalues are given by

$$r_{1,2} = \frac{\eta - \epsilon \pm \sqrt{(\eta+\epsilon)^2 - 4\,\epsilon\,\alpha}}{2}. \tag{6}$$

The fixed-point $(\bar{v}, \bar{w})$ is stable (unstable) for $\eta < \epsilon$ ($\eta > \epsilon$). There are two critical slopes given by

$$\eta_{cr}^{+} = -\epsilon + 2\sqrt{\epsilon\,\alpha} \qquad \text{and} \qquad \eta_{cr}^{-} = -\epsilon - 2\sqrt{\epsilon\,\alpha} \tag{7}$$

such that the eigenvalues are complex for $\eta \in (\,\eta_{cr}^{+}, \eta_{cr}^{-}\,)$ and real otherwise; i.e., the fixed point $(\bar{v}, \bar{w})$ is a focus for $\eta \in (\eta_{cr}^{-}, \eta_{cr}^{+})$ and a node otherwise. We show the corresponding stability diagram for $\epsilon = 0.01$ in Fig. 4-A. For a fixed value of α, as the slope of the linear piece η increases, the fixed point $(\bar{v}, \bar{w})$ changes from a stable node through stable and unstable spirals, to an unstable node. The horizontal line $\eta = \epsilon$ corresponds to the Hopf bifurcation points. As ϵ increases ("from red to blue" in Fig. 4-B) the Hopf bifurcation line moves upwards and the interval of values of η (range of slopes of the linear pieces) corresponding to the spiraling behavior widens.

The solution to system (4) for real eigenvalues r_1 and r_2 ($(\,\eta+\epsilon\,)^2 - 4\,\epsilon\,\alpha > 0$) is given by

$$\begin{bmatrix} v \\ w \end{bmatrix} \;=\; c_1 \begin{bmatrix} 1 \\ r_2 + \epsilon \end{bmatrix} e^{r_1 t} \;+\; c_2 \begin{bmatrix} 1 \\ r_1 + \epsilon \end{bmatrix} e^{r_2 t} \;+\; \begin{bmatrix} \bar{v} \\ \bar{w} \end{bmatrix} \tag{8}$$

with

$$c_1 = \frac{(v_0 - \bar{v})\,(r_1 + \epsilon) - (w_0 - \bar{w})}{r_1 - r_2} \qquad \text{and} \qquad c_2 = \frac{-(v_0 - \bar{v})\,(r_2 + \epsilon) + (w_0 - \bar{w})}{r_1 - r_2}. \tag{9}$$

In Fig. 4-C we show graphs of the real roots (r_1 and r_2) as a function of the slope of the linear pieces η for various values of α and $\epsilon = 0.01$. For $\eta < 0$ (left and right branches of the cubic-like PWL function) the corresponding fixed-point is stable (both eigenvalues are negative) while for $\eta > 0$ (middle branch of the cubic-like PWL function) the fixed-point is unstable (r_2 may become negative as η increases for small enough values of α). For small values of ϵ and large enough values of η there is a time scale separation (fast-slow system) which dissappears as η decreases or α increases.

The solution to system (5) for complex eigenvalues r_1 and r_2 ($(\,\eta+\epsilon\,)^2 - 4\,\epsilon\,\alpha < 0$) is given by

$$\begin{bmatrix} v \\ w \end{bmatrix} = c_1 \left[\begin{pmatrix} 1 \\ \beta \end{pmatrix} \cos\mu\,t \;+\; \begin{pmatrix} 0 \\ \mu \end{pmatrix} \sin\mu\,t \right] e^{r\,t} \;+$$

$$+\ c_2\ \left[\left(\begin{array}{c}1\\ \beta\end{array}\right)\ \sin\mu\,t\ -\ \left(\begin{array}{c}0\\ \mu\end{array}\right)\cos\mu\,t\right]\ e^{r\,t}\ +\ \left[\begin{array}{c}\bar{v}\\ \bar{w}\end{array}\right] \tag{10}$$

with

$$c_1 = v_0 - \bar{v}, \qquad\qquad c_2 = \frac{(v_0-\bar{v})\,(\eta+\epsilon) - 2\,(w_0-\bar{w})}{2\,\mu} \tag{11}$$

where

$$\mu = \sqrt{4\,\alpha\,\epsilon - (\eta+\epsilon)^2}\ /\ 2. \tag{12}$$

and

$$r = \frac{\eta-\epsilon}{2}, \qquad\qquad \beta = \frac{\eta+\epsilon}{2}. \tag{13}$$

In Fig. 4-D we show graphs of the natural frequency μ as a function of the slope of the linear piece for various values of α and $\epsilon = 0.01$.

3 The dynamics of $\mathbf{PWL}_{1,2,1}$ models of FHN-type

Here we investigate the mechanisms of generation of both small and large amplitude limit cycles and the abrupt transition between them (canard-like explosion) in $\mathrm{PWL}_{1,2,1}$ models of the form (2) where the cubic-like function $f_{pwl}(v)$ is as illustrated in Fig. 2. We show an example in Fig. 5 (panels A and B).

The middle branch of $f_{pwl}(v)$ has two linear pieces, L_1 and L_2, with slopes η_1 and η_2 respectively. We considered various representative values of the lengths and slopes of these linear pieces. The maximum and minimum of $f_{pwl}(v)$ are located at $(0,0)$ and $(1,1)$ respectively. As mentioned above, this canonical choice ensures that large amplitude oscillations are $\mathcal{O}(1)$. The left and right branches have one linear piece each, $L_{l,1}$ and $L_{r,1}$, with slopes $\eta_{l,1}$ and $\eta_{r,1}$ respectively. We used $\eta_{l,1} = \eta_{r,1} = -1$. As we will see, the number of pieces and the choice of slopes in both the left and right branches have little effect on the canard-like explosion for small enough values of ϵ.

In a $\mathrm{PWL}_{1,2,1}$ model, the two linear pieces in the middle branch (L_1 and L_2) join at the point $(\hat{v}_1, \hat{w}_1)$. For the example shown in Fig. 2, $(\hat{v}_1, \hat{w}_1) = (0.3, 0.09)$. From eqs. (5), if the intersection between the two nullclines, $N_w(v) = \alpha\,v - \lambda$ and $N_v(v) = f_{pwl}(v)$, occurs on the linear piece L_1, then the fixed point $(\bar{v}, \bar{w})$ is given by

$$\bar{v} = \frac{\lambda}{\alpha - \eta_1} \qquad \text{and} \qquad \bar{w} = \frac{\lambda\,\eta_1}{\alpha - \eta_1} \tag{14}$$

where η, $\hat{v}$ and $\hat{w}$ have been substituted by η_1, $\hat{v}_0 = 0$ and $\hat{w}_0 = 0$ in eqs. (5).

For $\lambda = 0$, $(\bar{v}, \bar{w}) = (0,0)$. As λ increases (decreases), the w-nullcline $N_w(v) = \alpha\,v - \lambda$ moves to the right (left), and so does the fixed point $(\bar{v}, \bar{w})$. This remains true if the intersection between the two nullclines occurs on the linear piece L_2. In this case, eq. (14) has to be modified accordingly.

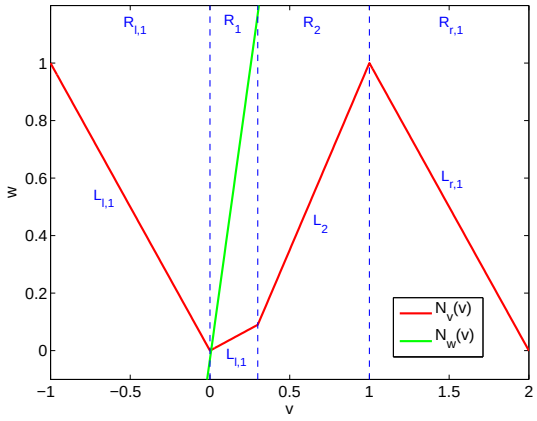

Figure 2: Nullclines (N_v and N_w), linear pieces and linear regimes for a $\text{PWL}_{1,2,1}$ cubic-like model (2) with $\alpha = 4$ and $\lambda = 0$. The slope of the linear pieces in N_v are (from left to right): $\eta_{l,1} = -1$ (left branch), $\eta_1 = 0.3$ and $\eta_2 = 1.3$ (middle branch), and $\eta_{r,1} = -1$ (right branch). The linear pieces in the middle branch join at $(\hat{v}_1, \hat{w}_1) = (0.3, 0.09)$.

	$(\hat{v}, \hat{w})$	η	r_1	r_2	r	μ		set
$L_{l,1}$	$(0, 0)$	-1.0	-0.052	-0.958			S - N	I
$L_{r,1}$		-1.0	-0.052	-0.958			S - N	I
L_1	$(0.3, 0.09)$	0.3			0.145	0.126	U - F	II
L_2	$(1, 1)$	1.3	1.269	0.021			U - N	II
L_1	$(0.4, 0.12)$	0.3			0.145	0.126	U - F	III
L_2	$(1, 1)$	1.467	1.439	0.018			U - N	III
L_1	$(0.9, 0.27)$	0.3			0.145	0.126	U - F	IV
L_2	$(1, 1)$	7.3	7.295	-0.045			U - N	IV

Table 1: $\text{PWL}_{1,2,1}$ models of FHN type for $\alpha = 4$ and $\epsilon = 0.01$. The parameters correspond to three models (sets I/II, sets I/III and sets I/IV) with the same left and right branches with a single linear piece each (set I). For each linear piece L_j, the table shows the right endpoints $(\hat{v}, \hat{w})$, the slope η, the eigenvalues of the corresponding linear regime (real eigenvalues r_1 and r_2, or real and imaginary parts, $r = (\eta - \epsilon)/2$ and μ respectively if the eigenvalues are complex). The transition from unstable foci (U-F) to unstable nodes (U-N) occurs at $\eta_{cr}^{+} = 0.39$. For the parameters we used, the transition from stable foci (S-F) to stable nodes (S-N) occur at $\eta_{cr}^{-} = -0.41$.

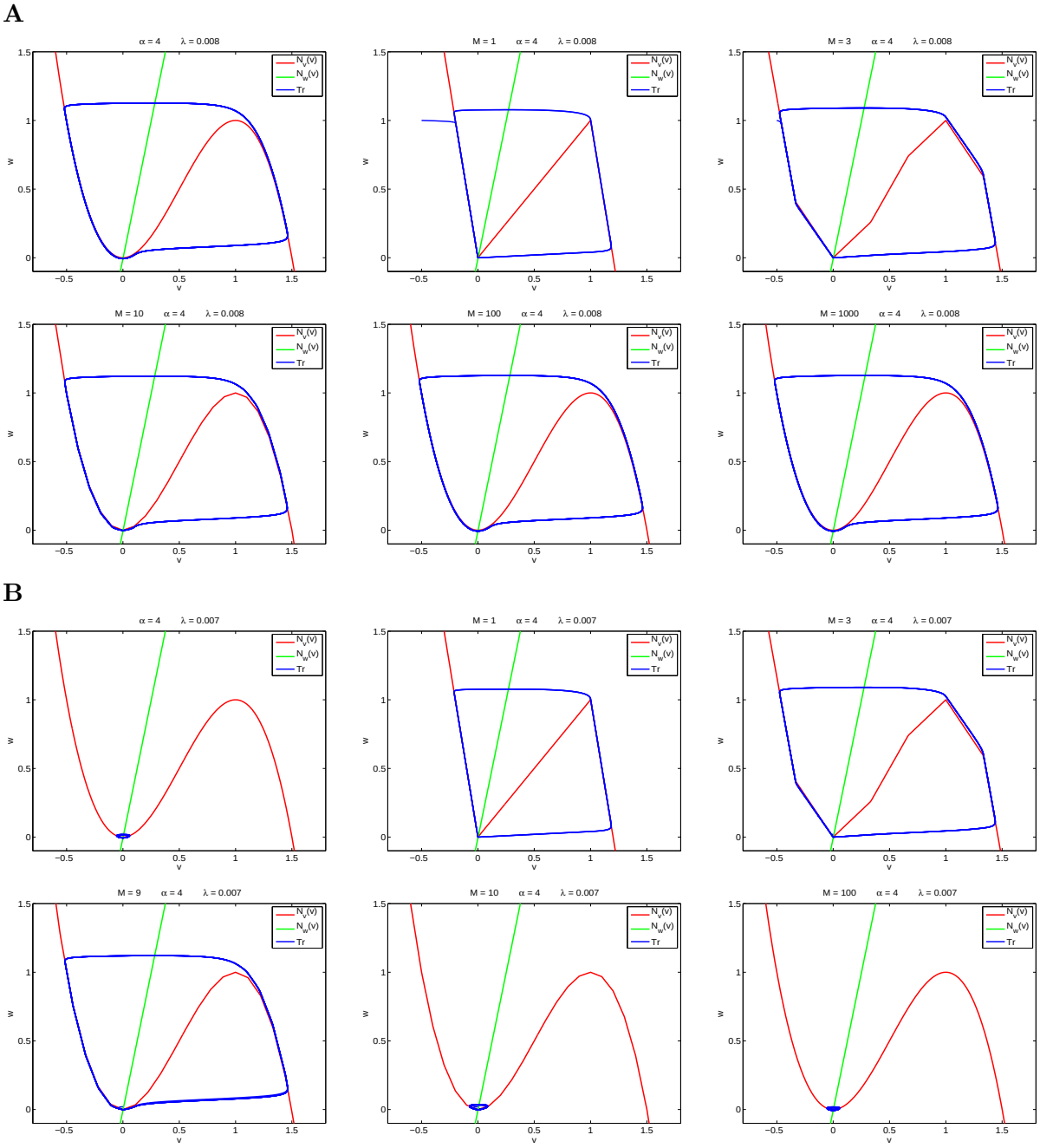

Figure 3: **Solutions to PWL$_M$ models approximate the corresponding smooth FHN model with $f(v) = -2\,v^3 + 3\,v^2$ as the number of linear pieces M increases. A:** $\lambda = 0.008$. **B:** $\lambda = 0.007$. The top-left panels in **A** and **B** show the phase-planes for the smooth FHN model in the relaxation oscillations and small amplitude oscillations regimes respectively. The corresponding values of λ are close to the canard critical point $\lambda_c \sim 0.0078$. As the number of linear pieces M increases (from the top-middle panel to the bottom-right panel) in both **A** and **B**, the solutions to the PWL$_M$ models approximate the solution to the smooth FHN model (shown in the top-left panel).

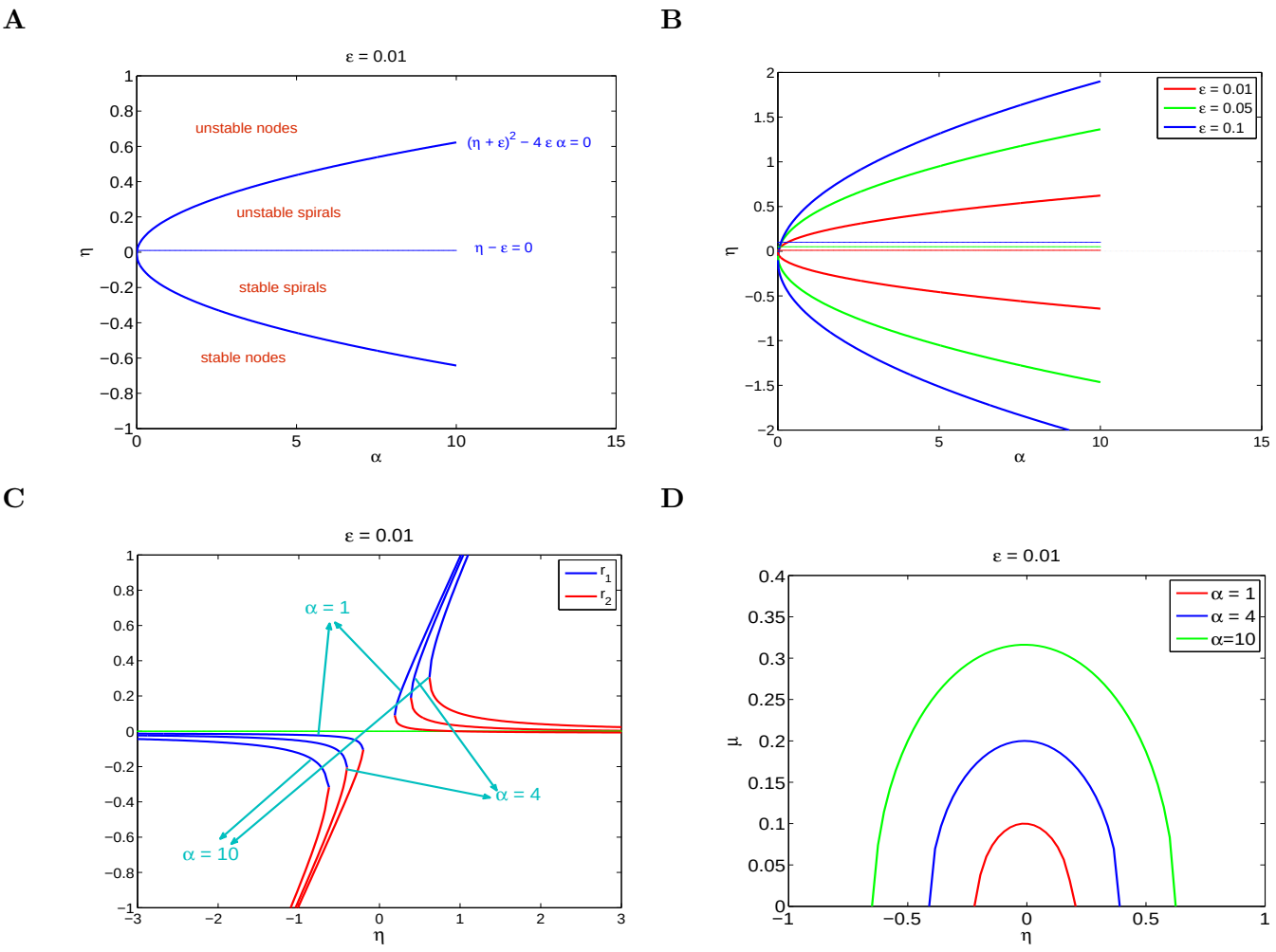

Figure 4: **Stability diagrams and eigenvalues for the basic linear components in a PWL model of FHN type. A** and **B.** Stability diagrams. For a fixed value of α, as η increases the fixed-point $(\bar{v}, \bar{w})$ changes from a stable node, through a stable and unstable focus, to an unstable node. **C.** Real eigenvalues (r_1 and r_2). They correspond to values of α and η satisfying $(\eta + \epsilon)^2 - 4\,\alpha\,\epsilon > 0$. **D.** Natural frequencies μ for complex eigenvalues. They correspond to values of α and η satisfying $(\eta + \epsilon)^2 - 4\,\alpha\,\epsilon < 0$.

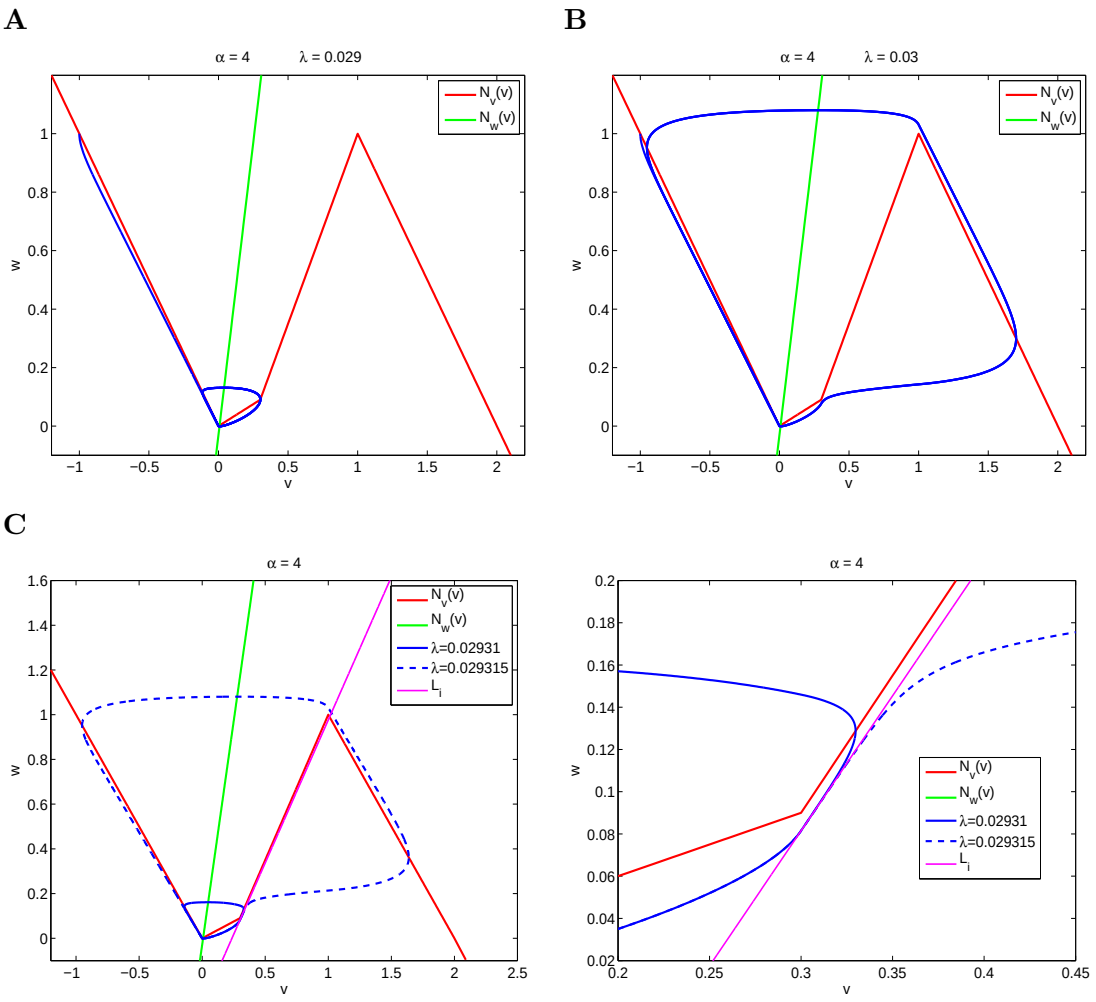

Figure 5: **Canard phenomenon in a PWL$_{1,2,1}$ model of FHN type. A.** Small amplitude limit cycle for $\lambda = 0.029$. **B.** Large amplitude limit cycle for $\lambda = 0.03$. **C.** Phase-plane diagram showing the inflection line L_1 (or $w = w_2(v)$) separating between a small amplitude limit cycle ($\lambda = 0.02931$) and a large amplitude limit cycle ($\lambda = 0.029315$). The inflection line is defined for values of $v \in [0.3, 1]$. For clarity, we extended it beyond this domain. The right panel is a magnification of the left one. We used $(v_1, w_1) = (0.3, 0.09)$, $\eta_1 = 0.3$, $\epsilon = 0.01$ and $\alpha = 4$. (See also Table 1, sets I and II).

For each linear piece, the eigenvalues are given by (6) with η substituted by the corresponding value of η_j. Eigenvalues and eigenvectors depend on the linear piece on which the fixed-point $(\bar{v}, \bar{w})$ is located but not on the precise location of the fixed-point on that linear piece; i.e., as λ increases, the eigenvalues and eigenvectors remain unchanged as long as the fixed point remains on the same linear piece. For future use, we present in Table 1 (sets I and II) the eigenvalues (r_1 and r_2), or their real and imaginary parts (r and μ) if they are complex, for the fixed-points in Fig. 2. Fixed-points located on the left and right branches are stable nodes ($r_1 < 0$ and $r_2 < 0$), fixed-points located on the linear piece L_1 are unstable foci ($r > 0$ and $\mu \neq 0$), and fixed-points located on the linear piece L_2 are unstable nodes ($r_1 > 0$ and $r_2 > 0$).

3.1 Assumptions and properties of the linear regimes

In $\text{PWL}_{1,2,1}$ systems, the linear regimes $\mathcal{R}_1$ and $\mathcal{R}_2$ satisfy some geometric and dynamic constraints. First, by construction, the slopes of L_1 and L_2 (linear pieces in the middle branch) and the v-coordinate $\hat{v}_1$ of the point joining them are related by

$$\eta_2 = \frac{1 - \eta_1 \, \hat{v}_1}{1 - \hat{v}_1}. \tag{15}$$

The exact form of this equation depends on our canonical choice of the maximum and minimum of $f_{pwl}(v)$. Similar expressions can be found for other values of (v_{min}, w_{min}) and (v_{max}, w_{max}) (see Section 2.1). Secondly, from (15), if $\eta_1 < 1$, then $\eta_2 > 1$. This also follows from geometric considerations. The slope of the line L joining the minimum $(0, 0)$ and maximum $(1, 1)$ of the cubic like $\text{PWL}_{1,2,1}$ function is $\eta = 1$. (This line would be the middle branch of a cubic-like $\text{PWL}_{1,1,1}$ function as the ones shown in Figs. 3-A and -B (top-left panels)). The two linear pieces L_1 and L_2 in Fig. 2 can be thought of as resulting from the line L "breaking" into two linear pieces with slopes smaller and larger than 1 (the slope of L) respectively.

Finally, the two regimes $\mathcal{R}_1$ and $\mathcal{R}_2$ have fixed-points with different stability properties. More specifically, if $\mathcal{R}_1$ has an unstable focus ($0 < \eta_1 < \eta_{cr}^+$ with $\eta_{cr}^+ \leq 1$), then $\mathcal{R}_2$ has an unstable node ($\eta_2 > \eta_{cr}^+$), and viceversa. (The critical slope η_{cr}^+ is given by the first equation in (7)). This is true since, by assuming the contrary ($\eta_2 \leq \eta_{cr}^+$), substituting in (15) and rearranging terms we arrive to $\eta_1 \geq \eta_{cr}^+$, contradicting our previous assumption. The converse is also true and follows from similar arguments by noting that eq. (15) holds if $\eta_1$and η_2 are exchanged.

We show in Section 3.6 that $\text{PWL}_{1,2,1}$ systems do not display small amplitude oscillations if $\mathcal{R}_1$ has an unstable node; i.e., a necessary (but not sufficient) condition for the occurrence of small amplitude oscillations is that $\mathcal{R}_1$ has a focus. Since the occurrence of the canard phenomenon requires the existence of small amplitude oscillations, here we consider parameters α, ϵ and η_1 satisfying $\eta_1 < \eta_{cr}^+$. We also require that $\eta_1 < \alpha$ in order to allow for the intersection between the linear piece L_1 and the w-nullcline ($N_w(v) = \alpha \, v - \lambda$) to occur for appropriate values of λ. In addition, we assume that the system has only one fixed-point.

Note that these assumptions are analogous to the requirement that the smooth system (1) undergoes a supercritical Hopf bifurcation. Consider the cubic function $f(v) = -hv^3 + av^2$ used in Fig.

1 ($h = 3$ and $a = 2$). As shown in Appendix A.4, for fixed values of h and a, there exists a critical value $\alpha_{crit} = 2a^2(3h)^{-1}$ such that the Hopf bifurcation is supercritical for $\alpha > \alpha_{crit}$ and subcritical for $\alpha < \alpha_{crit}$. As α decreases below α_{crit}, the smooth system loses its ability to generate stable small amplitude limit cycles. (For the choice of parameters in Fig. 1, $\alpha_{crit} = 3$). For a $\text{PWL}_{1,2,1}$ and a fixed value of η_1, since η_{cr}^+ is a decreasing function of α, a large enough decrease in the value of α causes η_{cr}^+ to decrease below η_1 thus changing the stability properties of the corresponding fixed-point of the linear regime $\mathcal{R}_1$ from an unstable focus to an unstable node and hence small amplitude oscillations are no longer possible (see Section 3.6).

3.2 Bifurcation structure

In Fig. 6-A we present the limit cycle amplitude diagram for the $\text{PWL}_{1,2,1}$ system corresponding to Fig. 2 and $\epsilon = 0.01$ as a function of the control parameter λ. Linear stability properties of fixed-points were determined as in section 2.3. Periodic solutions are constructed using the explicit formulas for trajectories given by the solutions in Section 2.3, matching continuously across sections where $v = \hat{v}_j$, and enforcing periodicity of solutions. These constraints generate a set of nonlinear algebraic equations which we solve numerically as in the earlier work by Coombes [22] to determine the period of solution, T, and the maximum and minimum values of the orbit.

For $\lambda < 0$, there is a stable node lying on the left branch of the v-nullcline (linear piece $L_{l,1}$). As λ increases, the fixed-point (14) moves to the right and crosses the minimum of the v-nullcline when $\lambda = 0$. For $0 < \lambda < 0.029$ the system has small amplitude limit cycles qualitatively similar to the ones shown in Fig. 5-A. The amplitudes of these limit cycles increase with λ. For $\lambda = 0.03$ the system has a large amplitude, relaxation type limit cycle (Fig. 5-B). A major difference between these small and large amplitude limit cycles is that trajectories cross the middle branch of the v-nullcline in the former while they don't, and move away from $\mathcal{R}_1$, in the latter. This is analogous to the smooth case.

With increasing values of ϵ it is possible for the branch of small amplitude oscillations to develop a fold so that stable small and large amplitude oscillations can coexist (and preclude the canard phenomenon). We illustrate this in Fig. 6-B. This phenomenon is not observed in smooth systems for the same parameter values ($\alpha = 4$ and $\epsilon = 0.1$). A similar folding in the PWL system occurs for other parameter sets as we illustrate in Fig. 7-A for $\alpha = 2$ and $\epsilon = 0.1$. However, differently from the $\alpha = 4$ case, for the $\alpha = 2$ case, the folding phenomenon persists in the corresponding smooth system Fig. 7-B.

The period of a small amplitude limit cycle is independent of λ

Here we show that for a periodic orbit like that shown in Fig. 5-A which visits only two distinct regimes $\mathcal{R}_1$ and $\mathcal{R}_2$ in the middle branch the period of the orbit is independent of λ.

The piecewise dynamical system (4) may be written in the form

$$z_j' = A_j z_j + b_j, \qquad z_j = \begin{bmatrix} v \\ w \end{bmatrix}, \quad (v, w) \in \mathcal{R}_j, \tag{16}$$

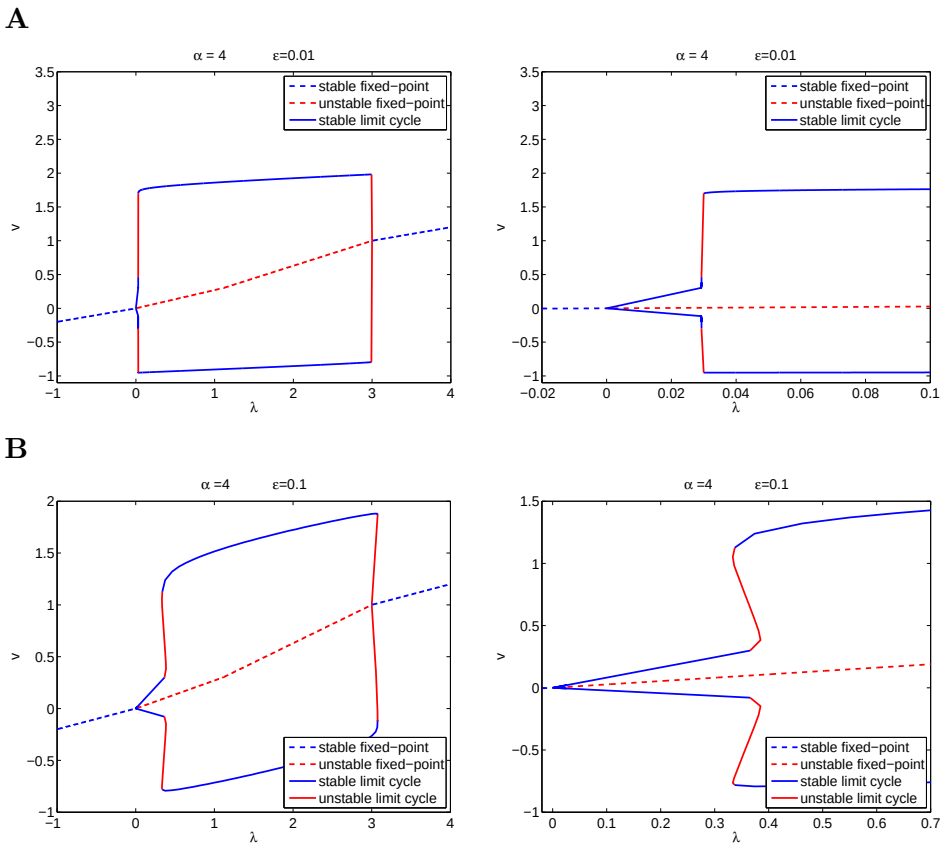

Figure 6: Bifurcation diagrams for the $\mathrm{PWL}_{1,2,1}$ model corresponding to Fig. 2 with $\epsilon = 0.01$ (**A**) and $\epsilon = 0.1$ (**B**). For fixed-points we present their v-coordinate. For periodic orbits we present the maximum and minimum values of their v-coordinate. The right panels are magnifications of the left ones.

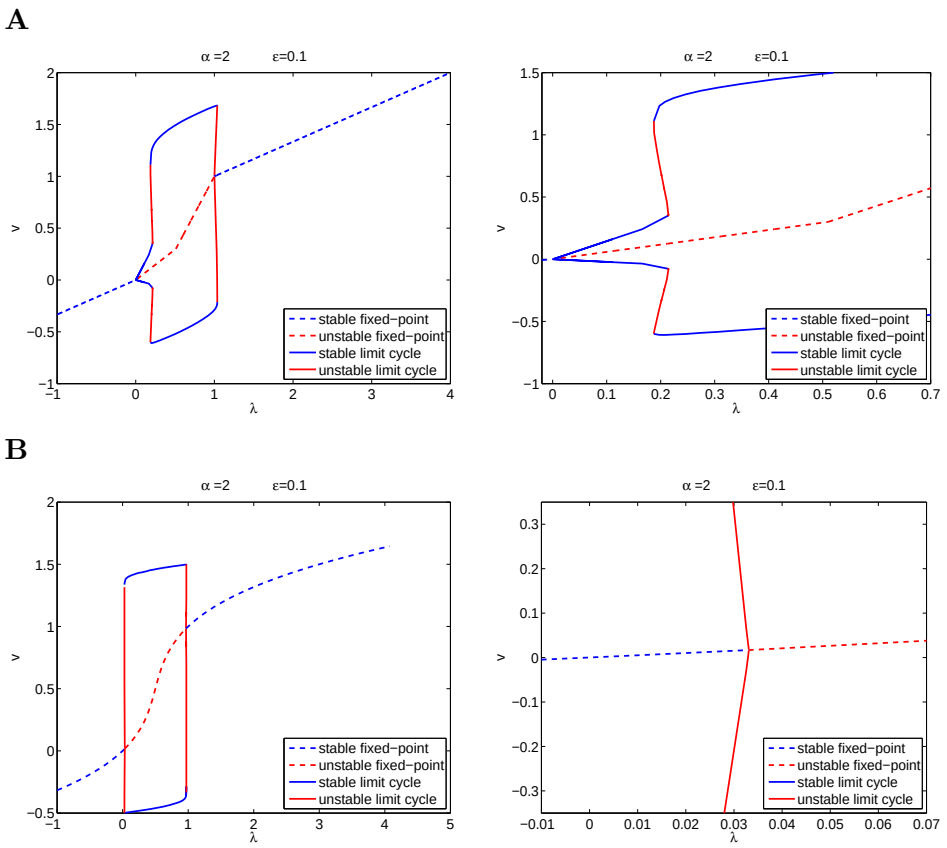

Figure 7: Comparison between the bifurcation diagrams for the $\mathrm{PWL}_{1,2,1}$ model (**A**) and the corresponding smooth FHN model (**B**) for $\alpha = 2$ and $\epsilon = 0.1$. For fixed-points we present their v-coordinate. For periodic orbits we present the maximum and minimum values of their v-coordinate. The right panels are magnification of the left ones.

where we use the index j to distinguish the dynamics of each linear regime. Here

$$A_j = \begin{bmatrix} \eta_j & -1 \\ \epsilon\alpha & -\epsilon \end{bmatrix}, \qquad b_j = \begin{bmatrix} -\eta_j \hat{v}_{j-1} + \hat{w}_{j-1} \\ -\epsilon\lambda \end{bmatrix}. \tag{17}$$

The solution to (16) may be written using matrix exponentials as

$$z_j(t) = G_j(t) z_j(0) + K_j(t) b_j, \qquad G_j(t) = \mathrm{e}^{A_j t}, \qquad K_j(t) = \int_0^t G_j(s) \mathrm{d}s. \tag{18}$$

Since the phase space is divided naturally into only two pieces we may without loss of generality set $(\hat{v}_1, \hat{w}_1) = (0, 0)$. We construct a periodic orbit by evolving a trajectory according to (18), with initial data $(v, w) = (0, w(0))$ (with $w(0)$ as yet undetermined), until $v = 0$ is reached again for the first time at $T_1 > 0$. We then evolve the trajectory with new initial data $(0, w(T_1))$ until meeting $v = 0$ again a time T_2 later. The "times-of-flight" T_j are determined by solving the threshold crossing conditions $v(T_1) = 0 = v(T_1 + T_2)$. A periodic solution can then be found by solving $w(T_1 + T_2) = w(0)$ for $w(0)$, yielding the period $T = T_1 + T_2$. For the special case that the trajectory only visits $\mathcal{R}_1$ and $\mathcal{R}_2$, b_j is independent of j and given by $b_j = -\epsilon\,\lambda\,(0, 1)^T$. Evolution from initial data $(0, w(0))$ to $(0, w(T_1))$ gives the pair of equations

$$G_2(T_1) \begin{bmatrix} 0 \\ w(0) \end{bmatrix} - \epsilon\lambda K_2(T_1) \begin{bmatrix} 0 \\ 1 \end{bmatrix} = \begin{bmatrix} 0 \\ w(T_1) \end{bmatrix}. \tag{19}$$

Dividing by $\epsilon\lambda$ means that we may solve for this pair of equations (say using Cramer's rule) in the form

$$\frac{w(0)}{\epsilon\lambda} = F_1(T_1), \qquad \frac{w(T_1)}{\epsilon\lambda} = F_2(T_1), \tag{20}$$

for some explicit functions $F_{1,2}$. A similar argument, with evolution of a trajectory from $(0, w(T_1))$ to $(0, w(0))$, gives

$$G_1(T_2) \begin{bmatrix} 0 \\ w(T_1) \end{bmatrix} - \epsilon\lambda K_1(T_2) \begin{bmatrix} 0 \\ 1 \end{bmatrix} = \begin{bmatrix} 0 \\ w(0) \end{bmatrix}. \tag{21}$$

Similarly we may solve for the pair $(w(0), w(T_1))$ as

$$\frac{w(0)}{\epsilon\lambda} = F_3(T_2), \qquad \frac{w(T_1)}{\epsilon\lambda} = F_4(T_2), \tag{22}$$

for some explicit functions $F_{3,4}$. Equating (20) and (22) gives two simultaneous equations for the pair (T_1, T_2):

$$F_1(T_1) = F_3(T_2), \qquad F_2(T_1) = F_4(T_2). \tag{23}$$

which are independent of λ. Hence $T = T_1 + T_2$ is independent of λ.

3.3 The mechanism of generation of small and large amplitude limit cycles and the abrupt transition between them

We begin by explaining the mechanisms that govern the generation of small and large amplitude limit cycles and the abrupt transition between both limit cycle amplitude regimes in the context of the

example presented in Fig. 5 as λ changes from 0.029 to 0.03. The parameters we used ($\eta_1 = 0.3$, $\alpha = 4$ and $\epsilon = 0.01$ with $\eta_{cr}^{+} = 0.39$) correspond to the supercritical canard phenomenon illustrated in Fig. 1-A for the smooth FHN system. As we progress in our discussion, we explain how changes in the values of these parameters affect the resulting dynamics. We will focus on changes in the relative lengths of L_1 and L_2, ϵ and α.

The dynamics of a $\text{PWL}_{1,2,1}$ system is divided into four linear regimes $\mathcal{R}_j$ corresponding to the four linear pieces L_j, and indexed accordingly (see Section 2.3) as shown in Fig. 2. The dynamics in each of these regimes are governed by a linear system of the form (4). The initial conditions for each regime $\mathcal{R}_j$ are equal to the values of v and w at the end of the previous regime (either R_{j-1} or R_{j+1}) as described in Section 2. Fig. 8-A shows the two trajectories in Fig. 5-A and -B ($\lambda = 0.029$ and $\lambda = 0.03$) in the same phase-plane. (The v-nullcline is independent of λ. The w-nullclines for both values of λ are indistinguishable. We plotted the w-nullcline corresponding to Fig. 5-A.) In these figures we have plotted the limit cycle trajectories after transients disappeared. These trajectories have been computed using the analytical solutions presented in Section 2.3. Alternatively, they can be computed numerically. Geometric and dynamic information corresponding to the four linear regimes are summarized in Table 1. We will refer to this table in our explanation.

As we mentioned in Section 1, the analytical solutions for PWL systems provide a poor insight into the models' dynamics. Below we use dynamical systems tools to explain these dynamics and answer various relevant questions about the abrupt transition between limit cycle amplitude regimes. In our explanation we investigate how limit cycle trajectories initially in the linear regime $\mathcal{R}_{l,1}$, near the left branch of the v-nullcline $L_{l,1}$, return to this regime after a cycle. One difficulty in investigating these limit cycle trajectories is that it is not possible to consider an initial point exactly on the limit cycle. We overcome this difficulty by computing an asymptotic approximation (for small values of ϵ) to the limit cycle trajectory in the linear regime $\mathcal{R}_{l,1}$ (see Appendix B.4). This is the trajectory we follow in our explanation and we will refer to it as the limit cycle trajectory although it is only an asymptotic approximation to the "real" limit cycle trajectory.

Linear regimes: virtual and actual fixed-points

A distinctive feature of PWL systems is that in each regime R_j dynamics are organized around a virtual fixed-point $(\bar{v}_j, \bar{w}_j)$ which results from the intersection between the w-nullcline $N_w(v) = \alpha\, v - \lambda$ and the linear piece L_j or its extension beyond the boundaries of R_j, $[\hat{v}_{j-1}, \hat{v}_j]$. In the latter case, virtual fixed-points are located outside the corresponding regime; i.e. $\bar{v}_j \notin [\hat{v}_{j-1}, \hat{v}_j]$. We illustrate this in Fig. 8-B for the linear regime $\mathcal{R}_{l,1}$. The vertical dashed lines separate between the linear regimes $\mathcal{R}_{l,1}$ and $\mathcal{R}_1$. The actual fixed-point $(\bar{v}, \bar{w})$ of the $\text{PWL}_{1,2,1}$ system (blue dot) is located on the intersection between the v- and w-nullclines (solid-red and -green lines respectively). The virtual fixed-point $(\bar{v}_{l,1}, \bar{w}_{l,1})$ for the linear regime $\mathcal{R}_{l,1}$ is located on the intersection between the extension of the linear piece $L_{l,1}$ (dotted-red line) and the w-nullcline which occurs in the linear regime $\mathcal{R}_1$ (and not in the linear regime $\mathcal{R}_{l,1}$). Clearly, the actual fixed-points $(\bar{v}, \bar{w})$ of a PWL system is also the virtual fixed-points for the regime where it is are located (see Fig. 9-B).

Within the boundaries of each regime, trajectories evolve as if the corresponding linear system,

which governs their dynamics as long as the trajectory is in that regime, govern their dynamics globally (for all values of t). In other words, within the boundaries of each regime trajectories evolve according to the linear dynamics defined in that regime and they "do not feel" that the dynamics governing their evolution will change at a future time when the trajectory moves to a different regime.

The dynamics in the linear regime $\mathcal{R}_{l,1}$

In Fig. 8-B we consider two trajectories initially located in the linear regime $\mathcal{R}_{l,1}$, close to the v-nullcline. The "blue" one is the limit cycle trajectory which evolves according to the $\text{PWL}_{1,2,1}$ system. It evolves in a small neighborhood of the v-nullcline due to the fast-slow nature of the system ($\epsilon = 0.01 \ll 1$). The "dotted-cyan" trajectory evolves according to the dynamics of the linear regime $\mathcal{R}_{l,1}$. It heads towards, and eventually converges to, the virtual fixed-point $(\bar{v}_{l,1}, \bar{w}_{l,1})$ (cyan dot) which is a stable node. (This follows from the analytic solution presented in Section 2.3. Since $\epsilon \ll 1$, it also follows from the asymptotic approximation to the slow manifold computed in Appendix B.4). For as long as the "blue" trajectory is in the linear regime $\mathcal{R}_{l,1}$ it evolves as the cyan one; i..e, as if it were attracted to the virtual fixed-point (cyan dot). This virtual fixed-point ceases to be the blue trajectory's target once this trajectory crosses the boundary between the linear regimes $\mathcal{R}_{l,1}$ and R_1 since its dynamics is no longer governed by the linear regime $\mathcal{R}_{l,1}$ but by the linear regime $\mathcal{R}_1$.

The dynamics in the linear regime $\mathcal{R}_1$

The dynamics of the trajectory in the linear regime $\mathcal{R}_1$ is shown in Fig. 9. This figure is a magnification of Fig. 8-A. The linear piece L_1 has slope $\eta_1 = 0.3 < \eta_{cr}^{+} = 0.39$. The dashed-red lines represent the extension of the linear piece L_1 beyond the boundaries of the linear regime $\mathcal{R}_1$. The corresponding fixed-point (blue dot) is an unstable focus (see Table 1) located on the intersection between L_1 (solid-red line) and the w-nullcline (green line) and is located in the linear regime $\mathcal{R}_1$. We show three trajectories in the right panel. The "solid-blue" and "dashed-blue" trajectories correspond to the small and large amplitude limit cycles shown in Fig. 8-A for $\lambda = 0.029$ and $\lambda = 0.03$ respectively. The "solid-blue" trajectory crosses the linear piece L_1 "almost" at the boundary between the linear regimes $\mathcal{R}_1$ and $\mathcal{R}_2$ and never enters $\mathcal{R}_2$. The "dashed-blue" trajectory crosses this boundary and moves into the linear regime $\mathcal{R}_2$. We address the dynamics of this trajectory in next section. The "dashed-cyan" trajectory initially coincides with the "solid-blue" trajectory and its evolution is governed (globally) by the linear regime $\mathcal{R}_1$. The left panel shows this "cyan" trajectory in the absence of the "blue" ones. Since the fixed-point is a focus, the "cyan" trajectory spirals out. (We only show the trajectory for the relevant time interval.) Once it enters the linear regime $\mathcal{R}_1$, the "solid-blue" trajectory also spirals out as if its dynamics were globally governed by this regime. The "solid-blue" and "cyan" trajectories split when they cross from $\mathcal{R}_1$ to $\mathcal{R}_{l,1}$. This has no consequences for the "cyan" trajectories which continues to spiral out. The dynamics of the "blue" trajectory, instead, ceases to be governed by that of $\mathcal{R}_1$ and returns to be governed by the linear regime $\mathcal{R}_{l,1}$. Consequently, it crosses the v-nullcline (solid-red line). The reminder of the dynamics are as explained above for the linear regime $\mathcal{R}_{l,1}$ (see Fig. 8).

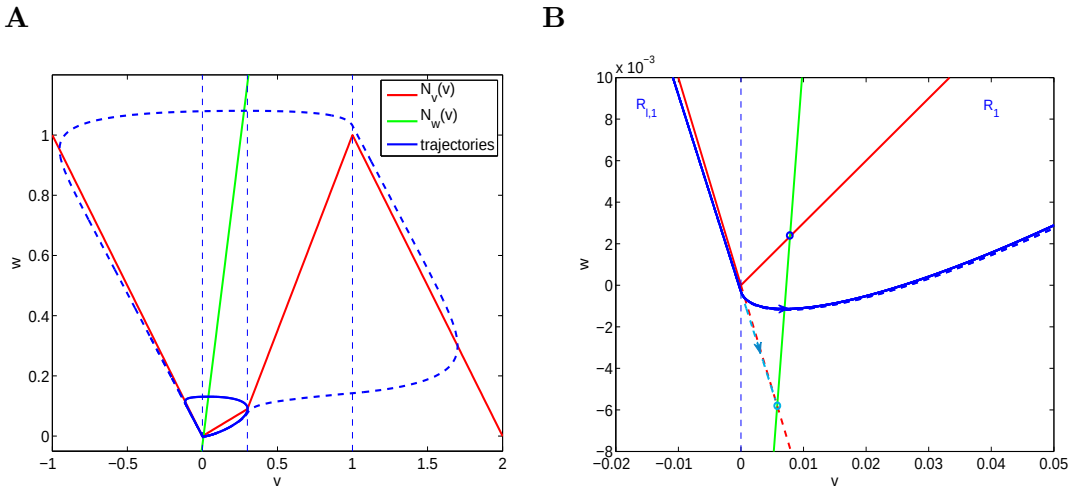

Figure 8: **Canard-like phenomenon in a PWL$_{1,2,1}$ model with $\alpha = 4$ and $\epsilon = 0.01$. Dynamics in the linear regime $\mathcal{R}_{l,1}$.** The nullclines are as in Fig. 2. The vertical (thin) dashed-lines separate between linear regimes and intersect the v-nullcline N_v at the joint points between the corresponding linear pieces. The actual fixed-point of the PWL$_{1,2,1}$ system is located in the linear regime R_1 and indicated with a blue dot (panel **B**) on the intersection between the two nullclines. **A.** Super-imposed trajectories for the small (solid) and large (dashed) amplitude limit cycles showed in Figs. 5-A and -B for $\lambda = 0.029$ and $\lambda = 0.03$ respectively. **B.** Dynamics of the trajectory in the linear regime $\mathcal{R}_{l,1}$. The dotted-red line indicates the continuation of the linear piece $L_{l,1}$ beyond the boundaries of the linear regime. The virtual fixed-point $(\bar{v}_{l,1}, \bar{w}_{l,1}) = (0.0058, -0.0058)$ for $\mathcal{R}_{l,1}$ is located in R_1 and indicated with a cyan dot (intersection between the dotted-red line and the w-nullcline N_w). The dotted-cyan curve corresponds to a trajectory whose global dynamics are governed by the linear regime $\mathcal{R}_{l,1}$ and shows that the virtual fixed-point is a stable node. Initially, this trajectory is located near the trajectory of the PWL$_{1,2,1}$ system (solid-blue). The slope of the linear pieces in N_v (from left to right) are: $\eta_{l,1} = -1$ (left branch), $\eta_1 = 0.3$ and $\eta_2 = 1.3$ (middle branch), and $\eta_{r,1} = -1$ (right branch). The linear pieces in the middle branch join at $(\hat{v}_1, \hat{w}_1) = (0.3, 0.09)$.

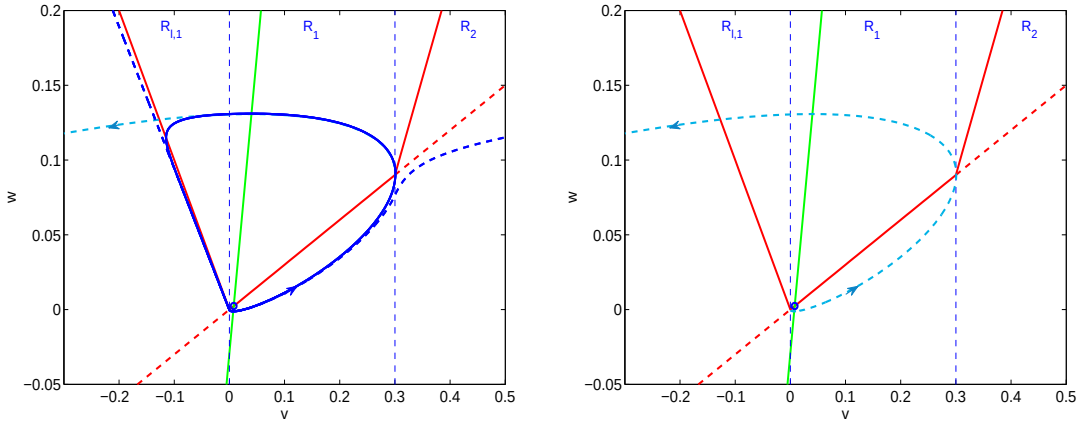

Figure 9: **Canard-like phenomenon in a PWL$_{1,2,1}$ model with $\alpha = 4$ and $\epsilon = 0.01$. Dynamics in the linear regime** R_1. This figure is a magnification of Fig. 8-A. The nullclines are as in Fig. 2. The solid-red PWL curve and the solid-green line represent the v- and w-nullclines (N_v and N_w) respectively. The vertical (thin) dashed-lines separate between linear regimes and intersect N_v at the joint points between the corresponding linear pieces. The dotted-red lines represent the continuation of the linear piece L_1 beyond the boundaries of the linear regime. The actual fixed-point $(\bar{v}, \bar{w}) = (0.0078, 0.0024)$ of the PWL$_{1,2,1}$ system is located in the linear regime $\mathcal{R}_1$ and indicated with a blue dot on the intersection between the two nullclines. The dotted-red lines indicates the continuation of the linear piece L_1 beyond the boundaries of the linear regime. The "dotted-cyan" curve corresponds to a trajectory whose global dynamics are governed by the linear regime $\mathcal{R}_1$ and illustrates that the fixed-point is an unstable focus. The "cyan" trajectory spirals out with frequency $\mu = 0.126$. The slope of the linear pieces in N_v (from left to right) are: $\eta_{l,1} = -1$ (left branch), $\eta_1 = 0.3$ and $\eta_2 = 1.3$ (middle branch), and $\eta_{r,1} = -1$ (right branch). The linear pieces in the middle branch join at $(\hat{v}_1, \hat{w}_1) = (0.3, 0.09)$.

The small amplitude limit cycle in Figs. 8 and 9 corresponds to a value of λ (= 0.029) for which the limit cycle trajectory intersects the v-nullcline in the linear regime $\mathcal{R}_1$ and never crosses to the linear regime $\mathcal{R}_2$. Limit cycle trajectories for smaller values of λ intersect the linear piece L_1 at lower values of v (not shown). These values of v depend on the amplitude of the initial oscillation of the trajectory after entering the linear regimes $\mathcal{R}_1$ (see solid-blue trajectory in Fig. 9). This amplitude, in turn, depends on the distance

$$D = D(w_0, \lambda) = D(w_0, \bar{v}_1, \bar{w}_1) = \sqrt{(v_0 - \bar{v}_1)^2 + (w_0 - \bar{w}_1)^2} \tag{24}$$

between the initial point $(v_0, w_0) = (0, w_0)$ in $\mathcal{R}_1$ and the fixed-point $(\bar{v}_1, \bar{w}_1) \in \mathcal{R}_1$, parametrized by λ, through the constants c_1 and c_2 (11) in the solution (10) presented in Section 2.3. (This parametrization is well defined since we assumed that for each value of λ there is a unique fixed-point.) Note that in (24) $v_0 = 0$ and $\bar{w}_1 = \eta_1 \bar{v}_1$. To leading order, the initial value w_0 can be analytically approximated using the asymptotic computation in Appendix B.4. For $\epsilon \ll 1$, $w_0 = \mathcal{O}(\epsilon)$.

For $\lambda = 0$, $D = 0$ since $(\bar{v}_1, \bar{w}_1) = (0, 0)$ is a stable node. In Section 3.5 we show that D is an increasing function of λ. For a fixed value of the length of the linear piece L_1, if D is small enough, then the trajectory crosses L_1 as it occurs in Figs. 8 and 9 for the "solid-blue" trajectory. On the other hand, if D, and hence λ, is large enough, then the trajectory reaches the boundary between the linear regimes $\mathcal{R}_1$ and $\mathcal{R}_2$ without crossing the linear piece L_1 as it occurs in Figs. 8 and 9 for the "dashed-blue" trajectory. Once the trajectory crosses this boundary its dynamics ceases to be goverend by the linear regime $\mathcal{R}_2$ and turns to be governed by the linear regime $\mathcal{R}_2$.

The dynamics in the linear regime $\mathcal{R}_2$

The dynamics of the trajectory in the linear regime $\mathcal{R}_2$ is shown in Fig. 10. The linear piece L_2 has slope $\eta_2 = 1.3 > \eta_{cr}^+ = 0.39$. The corresponding virtual fixed-point (blue dot) is an unstable node (see Table 1) located on the intersection between the extension of the linear piece L_2 (dashed-red lines) and the w-nullcline (green line) and is located in the linear regime $\mathcal{R}_{l,1}$ (not in $\mathcal{R}_2$). As in the previous figures, we show three types of trajectories. The "solid-blue" and "dashed-blue" trajectories correspond to the small and large amplitude limit cycles shown in Fig. 8-A for $\lambda = 0.029$ and $\lambda = 0.03$ respectively. Their dynamics are governed by the $\text{PWL}_{1,2,1}$ system. Both evolve very close in the linear regimes $\mathcal{R}_{l,1}$ and $\mathcal{R}_1$ and bifurcate near the boundary between these two linear regimes. The two "dashed-cyan" trajectories evolve according the dynamics of the linear regime $\mathcal{R}_2$ for all values of t. They are initially located near the virtual fixed-point and the "dashed-blue" trajectory respectively. They move fast along almost horizontal direction as expected from fast-slow systems. They illustrate the fact that the virtual fixed-point is an unstable node (see Table 1, set II).

The "dashed-blue" trajectory eventually crosses the boundary between the linear regimes $\mathcal{R}_2$ and $\mathcal{R}_{r,1}$ and its dynamics changes accordingly.

The dynamics in the linear regime $\mathcal{R}_{r,1}$

The dynamics of the trajectory in the linear regime $\mathcal{R}_{r,1}$ is shown in Fig. 11. It is qualitatively similar to the dynamics on the linear regime $\mathcal{R}_{l,1}$. The linear piece $L_{r,1}$ has slope $\eta_{r,1} = -1$. The

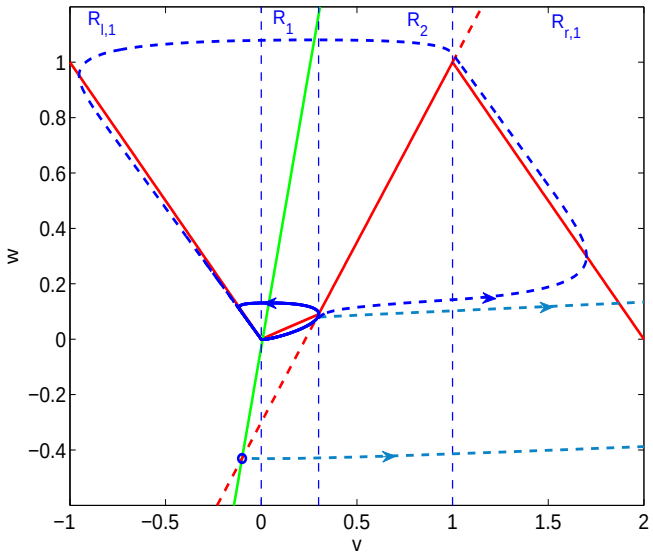

Figure 10: **Canard-like phenomenon in a PWL$_{1,2,1}$ model with $\alpha = 4$ and $\epsilon = 0.01$. Dynamics in the linear regime** R_2. The nullclines are as in Fig. 2. The solid-red PWL curve and the green line represent the v- and w-nullclines (N_v and N_w) respectively. The vertical (thin) dashed-lines separate between linear regimes and intersect N_v at the joint points between the corresponding linear pieces. The dotted-red lines represent the continuation of the linear piece L_2 beyond the boundaries of the linear regime. The virtual fixed-point $(\bar{v}_2, \bar{w}_2)$ is located in $\mathcal{R}_{l,1}$ and indicated with a blue dot (intersection between the dotted-red line and the w-nullcline N_w). The dashed-cyan curves correspond to trajectories whose global dynamics are governed by the linear regime R_2 and illustrate that the fixed-point is an unstable node. Initially, the two cyan curves are located near the virtual fixed-point and near the trajectory of the PWL$_{1,2,1}$ system (solid-blue curve) respectively. The slope of the linear pieces in N_v (from left to right) are: $\eta_{l,1} = -1$ (left branch), $\eta_1 = 0.3$ and $\eta_2 = 1.3$ (middle branch), and $\eta_{r,1} = -1$ (right branch). The linear pieces in the middle branch join at $(\hat{v}_1, \hat{w}_1) = (0.3, 0.09)$.

corresponding virtual fixed-point (blue dot) is located on the intersection between the extension of the linear piece $L_{r,1}$ (dashed-red line) and the w-nullcline (green line) and is located in the linear regime $\mathcal{R}_2$. In the left panels we show the trajectories of the $\text{PWL}_{1,2,1}$ system (using the same notation). For clarity, in the right panel we show only trajectories whose dynamics are governed (globally) by the linear regime $\mathcal{R}_{r,1}$. This illustrates that the virtual fixed-point is a stable node (see also Table 1, set I). The "dashed-blue" trajectory crosses the linear piece $L_{r,1}$ and continues to evolve in a close vicinity of it heading towards the virtual fixed-point. When the trajectory crosses the boundary between the linear regimes $\mathcal{R}_{r,1}$ and $\mathcal{R}_2$ its dynamics ceases to be governed by the linear regime $\mathcal{R}_{r,1}$ and, consequently, the virtual fixed-point ceases to be the trajectory's target. The reminder of the dynamics of the limit cycle trajectory is standard for relaxation oscillators and can be explained using the same ideas explained above.

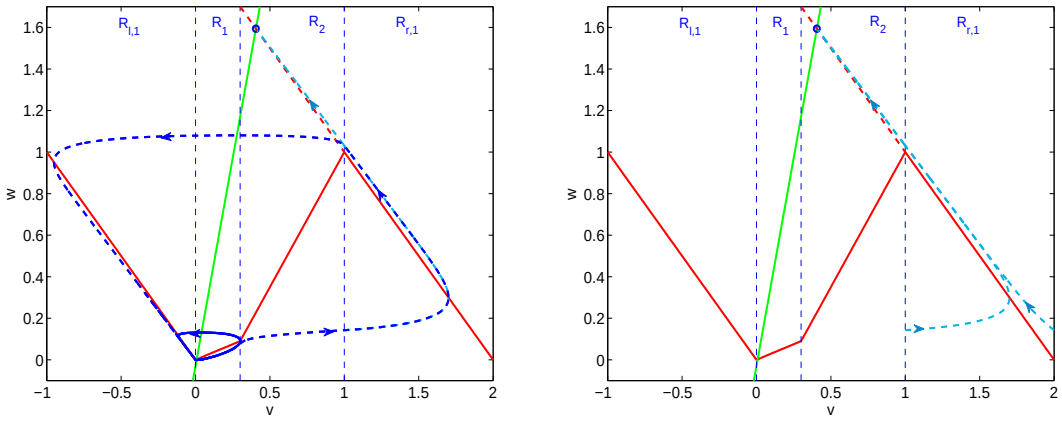

Figure 11: **Canard-like phenomenon in a $\text{PWL}_{1,2,1}$ model with $\alpha = 4$ and $\epsilon = 0.01$. Dynamics in the linear regime** $R_{r,1}$. The nullclines are as in Fig. 2. The vertical (thin) dashed-lines separate between linear regimes and intersect the v-nullcline N_v at the joint points between the corresponding linear pieces. The dotted-red lines indicates the continuation of the linear piece $L_{r,1}$ beyond the boundaries of the linear regime. The virtual fixed-point $(\bar{v}_{r,1}, \bar{w}_{r,1})$ is located in R_2 and indicated with a blue dot (intersection between the dotted-red line and the w-nullcline N_w). The dotted-cyan curves correspond to trajectories whose global dynamics are governed by the linear regime $R_{r,1}$ and illustrate that the fixed-point is a stable node. Initially, the cyan curves are located near and away from the trajectory of the $\text{PWL}_{1,2,1}$ system (solid-blue) respectively. The slope of the linear pieces in N_v (from left to right) are: $\eta_{l,1} = -1$ (left branch), $\eta_1 = 0.3$ and $\eta_2 = 1.3$ (middle branch), and $\eta_{r,1} = -1$ (right branch). The linear pieces in the middle branch join at $(\hat{v}_1, \hat{w}_1) = (0.3, 0.09)$.

Together, the results in this section provide a geometric and dynamic picture of how the canard-like explosion occurs in $\text{PWL}_{1,2,1}$ systems that can be extended to other parameter regimes. To a first approximation, a small amplitude limit cycle is created if the amplitude of the initial spiraling out

oscillation in the linear regime $\mathcal{R}_1$ is small enough for the trajectory to be able to cross the linear piece L_1 and a large amplitude oscillation is created otherwise. This initial amplitude depends on both λ and the properties (length and slope) of the linear piece L_1. The dependence of λ occurs through the distance between the trajectory's initial point in the linear regime $\mathcal{R}_1$ and the fixed-point. For all other parameters fixed, an increase in the value of λ causes increase in this initial distance and, in turn, causes the amplitude of the small amplitude limit cycle to increase until, for some critical value of λ, the trajectory cannot longer cross the linear piece L_1. We analyze the effects of changes in the model parameters on the canard-like phenomenon later in this paper.

An important aspect of these dynamics, highlighted by our results, is that trajectories evolve in a close vicinity of the unstable (middle) branch of the cubic-like function for a significant amount of time, as it occurs for smooth systems, not because they are attracted to it nor because they are not repelled enough. They are indeed repelled but in a spiraling-out manner. For small amplitude oscillations, this repulsion ceases when the trajectory returns to the vicinity of the slow manifold (left branch). For large amplitude oscillations, the repulsion continues once the trajectories enter the linear regime $\mathcal{R}_2$ but it changes from "focus-like" to "node-like" which enables the trajectory to move fast away from the fixed-point towards the right branch of the PWL function.

Inflection lines and eigenvectors

For $\epsilon \ll 1$, between small and large amplitude limit cycles there exists an orbit with a point of inflection [35, 36, 37] (see Appendix B.5). This generates a curve (line) in phase-plane dividing between regions of small and large amplitude limit cycle oscillations as we show in Fig. 5-C. We derive the inflection lines L_{infl} in Appendix B.5. For the linear system governing the dynamics in $\mathcal{R}_2$ the inflection lines are given by

$$L^{1,2}_{infl}(v) = \alpha\,\frac{\eta - r_{1,2} - \epsilon}{\alpha - r_{1,2} - \epsilon}\,v + \frac{\lambda\,(r_{1,2}+\epsilon) - \alpha\,(\eta\,\hat{v} - \hat{w})}{\alpha - r_{1,2} - \epsilon} \tag{25}$$

where $r_{1,2}$ are the eigenvalues (6) of the system in $\mathcal{R}_2$, η is the slope of L_2 and $(\hat{v}, \hat{w})$ are the left end-point of L_2 $(\hat{v}_1, \hat{w}_1)$. In Fig. 5-C we present the inflection lines corresponding to the transition between the small and large amplitude limit cycles ($\lambda = \lambda_c$). In Appendix B.6 we show that the inflection lines coincide with the "eigenvector lines" $W_{2,1}(v)$

$$W_{2,1}(v) = (\,r_{2,1} + \epsilon\,)\,v - (\,r_{2,1} + \epsilon\,)\,\bar{v} + \bar{w} \tag{26}$$

that have the eigenvector directions and cross the virtual fixed-point $(\bar{v}_2, \bar{w}_2)$ of the system. Note that for $\epsilon = 0$ both lines coincide with the v-nullcline.

3.4 The canard critical value λ_c

In smooth systems, the canard phenomenon occurs for a range of values of λ which is exponentially small in ϵ. Within this small critical range, as λ increases, the amplitude of the limit cycle increases between these values corresponding to the small and large amplitude oscillations regimes, and the

limit cycle trajectory is able to move in a close vicinity of the unstable branch of the v-nullcline for a significant amount of time (see Fig. 1-A). There is a value of λ within this critical range that corresponds to the so called maximal canard. This value of λ is typically used to define the canard critical value λ_c. However, maximal canards are typically not observable in realistic situations and the exact value of λ_c is difficult to compute. Approximations to λ_c have been obtained (see discussion in Appendix A.2). These approximations can be thought of as approximations to the critical range over which the abrupt transition occurs, and are useful to predict whether a smooth system will display either small or large amplitude oscillations with a high degree of accuracy.

Following these ideas for smooth systems, we provide here a working definition of the canard critical value λ_c for PWL systems as the value of λ separating between small and large limit cycle amplitude regimes, and we provide a method for approximating λ_c, and the critical range over which the abrupt transition occurs, that allows to make quantitative predictions.

For the parameters in Fig. 5 (and Figs. 8 to 11), to a first approximation, limit cycles have small amplitude for $\lambda \leq 0.029$ and large amplitude for $\lambda \geq 0.03$. In addition, $\lambda = 0.029$ has been graphically identified as the"last" value of λ for which the limit cycle trajectory crosses the linear piece L_1; i.e., the intersection between the limit cycle trajectory and the v-nullcline approximately occurs at the joint point between the linear pieces L_1 and L_2, and a very small increase in the value of λ generates a large amplitude limit cycle. A closer examination shows that small amplitude limit cycles can cross the linear piece L_2 for values of $\lambda \in (0.029, 0.02931)$ as we show in Fig. 5-C. However, the range of values of λ for which this occurs (0.00031) is small as compared to $\lambda = 0.029$, so choosing $\lambda = 0.029$ as the critical value of λ for which the abrupt transition between small and large amplitude limit cycles occurs (canard-like phenomenon) provides a good approximation to the "real" critical value defined above.

Generalizing these ideas, we approximate the canard critical value by the value of λ for which the limit cycle trajectory intersects the middle branch of the v-nullcline at the joint point between the linear pieces L_1 and L_2. (This is the "last" value of λ for which limit cycle trajectories do not cross from $\mathcal{R}_1$ to $\mathcal{R}_2$.) Similarly to the approximations to the canard critical value for smooth systems discussed above (and in Appendix A), we will use the symbol λ_c and the term canard critical value to refer to this approximation. For the parameters in Figs. 5, comparison of this value ($\lambda_c = 0.029$) with the more accurate one in Fig. 5-C ($\lambda = 0.0293125$) where small amplitude limit cycle trajectories are able to cross to $\mathcal{R}_2$ yields a relative error equal to 0.01069 (1.069%). (The value $\lambda = 0.0293125$ has been numerically calculated as the mean between the values of λ corresponding to the "last" small and "first" large amplitude oscillations. Note that the relative error is of the same order of magnitude as $\epsilon = 0.01$.)

The canard critical value λ_c increases with the size of L_1

We illustrate this in Fig. 12 where all the parameters are the same as in Fig. 5 with the exception of $|L_1|$, that is larger in Fig. 12 than in Fig. 5. In particular, the slope $\eta_1 = 0.3$ is the same in Figs. 12 and 5. From eq. (15), the slope of L_2 ($\eta_2 = 1.467$) is larger in Fig. 12 than in Fig. 5. From our discussion in Section 3.1, the stability properties of the virtual fixed-points in both $\mathcal{R}_1$ and $\mathcal{R}_2$ do not

change as $|L_1|$ increases; they are an unstable focus and unstable node regimes respectively. (Note that since α and ϵ are the same for both figures so is η_{cr}^{+}).

In Fig. 12-A, $\lambda = 0.03$. In contrast to Fig. 5-B, the trajectory is able to cross the linear piece L_1 in Fig. 12-A because of the increased length of L_1. Thus the system has a small amplitude limit cycle for a value of λ for which Fig. 5-A shows a large amplitude limit cycle. Only when λ increases to $\lambda = 0.039$, corresponding to $(\bar{v}_1, \bar{w}_1) = (0.0105, 0.0032)$, does the canard explosion occur. Similarly to Fig. 5, the virtual fixed-point $(\bar{v}_2, \bar{w}_2) = (-0.17, -0.71)$ in $\mathcal{R}_2$ is an unstable node so the trajectory moves away from $\mathcal{R}_1$ and generates a large amplitude limit cycle (Fig. 12-B). The canard explosion in this case occurs for values of $\lambda \in (0.038, 0.039)$ and can be approximated by $\lambda_c = 0.038$. As λ increases further, $D(w_0, \lambda)$ also increases, and the limit cycle approaches a fully developed relaxation oscillator (Fig. 12-C).

These ideas can be generalized. For a given set of parameters $(\alpha, \epsilon, \eta_1)$, λ_c depends on the initial amplitude $D(w_0, \lambda)$ of the limit cycle trajectory in $\mathcal{R}_1$, given by eq. (24), and $|L_1|$. In Appendix B.4 we show that for $\epsilon \ll 1$, to a first approximation, initial conditions in $\mathcal{R}_1$ are independent of λ (they differ in $\mathcal{O}(\epsilon)$). Then, for $\epsilon \ll 1$, the initial distance $D(w_0, \lambda)$ is independent of w_0, and λ_c depends only on the location of the fixed point $(\bar{v}_1, \bar{w}_1)$, parametrized by λ (14), and $|L_1|$. As λ increases, the fixed-point moves to the right, $D(w_0, \lambda)$ increases, and the limit cycle trajectory intersects the v-nullcline N_v at a "higher" point until this intersection no longer occurs in $\mathcal{R}_1$. As before, we take an approximation to λ_c as the maximum value of λ for which the trajectory intersects the linear piece L_1 at its joint point with the linear piece L_2. For all other parameters fixed, as $|L_1|$ increases, the range of values of λ for which limit cycle trajectories and N_v intersect in $\mathcal{R}_1$ also increases, and so does λ_c.

In principle, the mechanism described here works for linear pieces L_1 with arbitrary lenghts $|L_1| < (1 + \eta_1^2)^{1/2}$ (within the boundaries of the middle branch). However, the technically small amplitude limit cycles created by long linear pieces L_1 may not lead to small amplitude oscillations; i.e., to oscillations whose amplitude is an order of magnitude smaller than these created by large amplitude limit cycles. We illustrate this in Fig. 12-D and -E for a linear piece L_1 with right endpoint $\hat{v}_1 = 0.9$. The canard-like explosion still occurs for $\lambda \in (0.0868, 0.0869)$ but the limit cycle amplitudes in both regimes are roughly of the same order of magnitude.

Effects of changes in ϵ on the canard-like phenomenon and λ_c

The canard phenomenon described above occurs because limit cycle trajectories are able to cross the middle (unstable) branch of the v-nullcline for values of $\lambda < \lambda_c$ while they are not able to do so for larger values of λ. This is the result of two different features of the system: the time scale separation ($\epsilon \ll 1$) and the cubic-like nonlinearities, in particular the fact that the middle branch breaks into two linear pieces with different stability properties, unstable focus ($\mathcal{R}_1$) and node ($\mathcal{R}_2$) respectively. The time scale separation is responsible for "forcing" trajectories to move away from the linear piece L_2 (in the linear regime $\mathcal{R}_2$) thus preventing trajectories from crossing L_2 to create a small amplitude limit cycle. The result is a large amplitude limit cycle.

In order to further understand the effect of time scale separation on the canard-like phenomenon, we show in Fig. 13 the phase-diagrams for two representative values of ϵ (larger than the one we

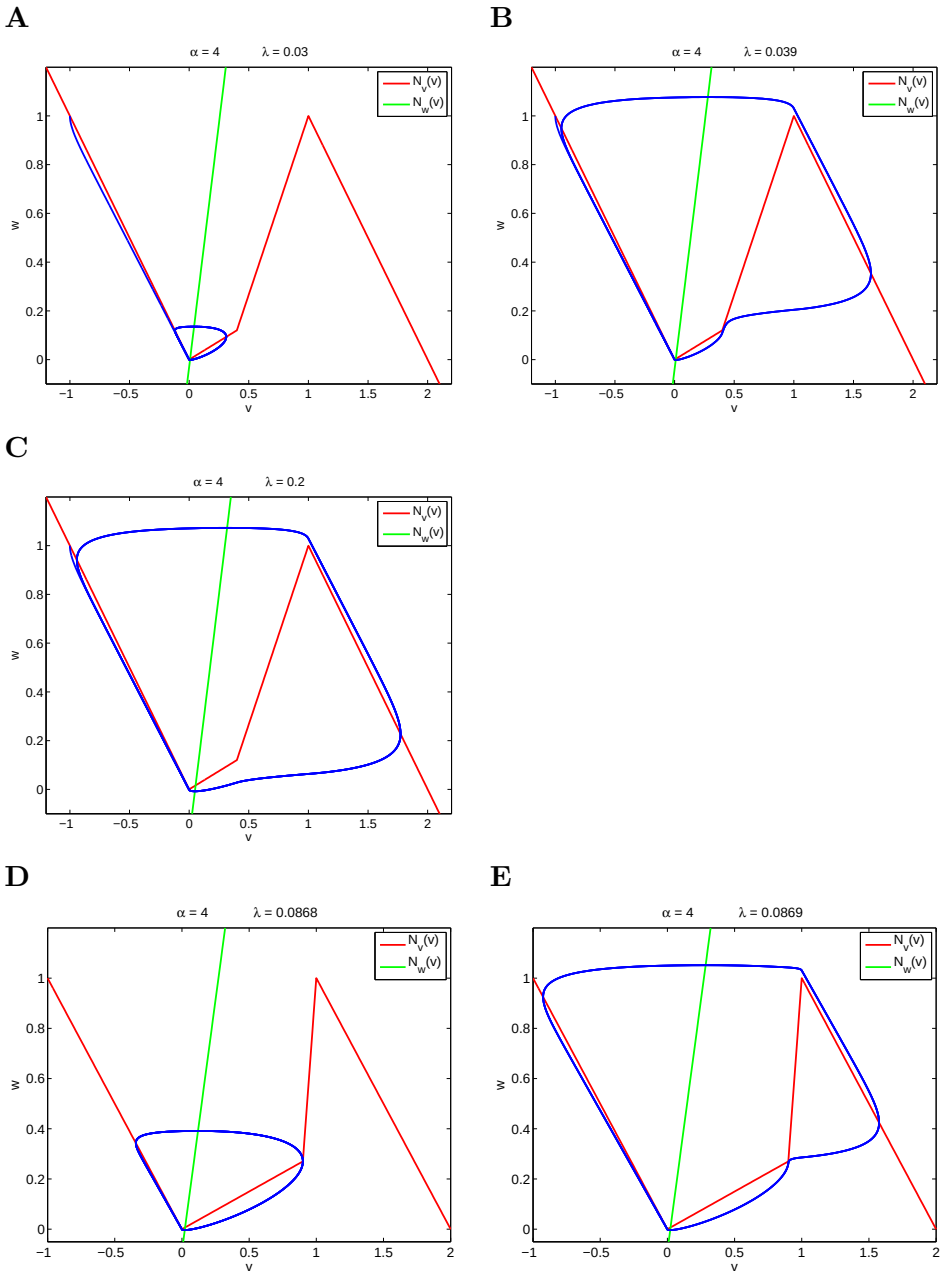

Figure 12: **Canard phenomenon in a PWL$_{1,2,1}$ model of FHN type.** We used $\eta_1 = 0.3$, $\epsilon = 0.01$ and the parameters presented in Table 1 (sets I, III and IV). **A** Small amplitude limit cycle for $\lambda = 0.03$, $v_1 = 0.4$ and the parameters presented in Table 1 (sets I and III). **B** Large amplitude limit cycle for $\lambda = 0.039$, $v_1 = 0.4$ and the parameters presented in Table 1 (sets I and III). **C** Large amplitude limit cycle for $\lambda = 0.2$, $v_1 = 0.4$ and the parameters presented in Table 1 (sets I and III). **D** Small amplitude limit cycle for $v_1 = 0.9$, $\lambda = 0.0868$ and the parameters presented in Table 1 (sets I and IV). **E** Large amplitude limit cycle for $v_1 = 0.9$, $\lambda = 0.0869$ and the parameters presented in Table 1 (sets I and IV).

considered so far): $\epsilon = 0.1$ (panels A) and $\epsilon = 0.3$ (panels B). For $\epsilon = 0.1$, although the time scale separation is smaller than for $\epsilon = 0.01$, the transition between amplitude regimes is still abrupt. It occurs for values of $\lambda \in (0.385, 0.3852)$. Although this interval is larger than $(0.02931, 0.029315)$ (the corresponding interval for $\epsilon = 0.01$), it is still very small. In this case, $\lambda_c = 0.385$ which is larger than the critical value for $\epsilon = 0.01$. As expected, the shapes of the limit cycles differ from those in Fig. 5. The limit cycle trajectories evolve further away from the v-nullcline than for $\epsilon = 0.01$ and the large amplitude limit cycle trajectory does not move almost horizontally in the linear regime $\mathcal{R}_2$ as happens for $\epsilon = 0.01$. The stability properties for the two cases ($\epsilon = 0.01$ and $\epsilon = 0.1$) have similarities and differences. Similarly to the $\epsilon = 0.01$ case, the fixed-points for $\epsilon = 0.1$ in the linear regimes $\mathcal{R}_1$ and $\mathcal{R}_2$ (middle branches) are unstable foci and nodes respectively (not shown). In contrast to the $\epsilon = 0.01$ case, the virtual fixed-points in the linear regimes $\mathcal{R}_{l,1}$ and $\mathcal{R}_{r,1}$ (left and right branches respectively) are stable focus rather than stable nodes (not shown). This does not qualitatively change the basic mechanism explained in Section 3.3.

For $\epsilon = 0.3$ (Fig. 13-B), the transition from small to large amplitude limit cycles is much less abrupt and occurs on a larger range of values of λ over which trajectories are able to cross the linear piece L_2. Associated with the abrupt transition in Fig. 13-A for $\epsilon = 0.1$, there is the inflection of the trajectory as it crosses from the linear regime $\mathcal{R}_1$ to $\mathcal{R}_2$. This inflection is absent for $\epsilon = 0.3$ in Fig. 13-B.

3.5 Analytical approximation of the canard critical point

Here we show that given α, $\epsilon \ll 1$, η_1 (slope of L_1), $\hat{v}_1$ (joint point between L_1 and L_2), and the initial value w_0, one can predict to a good degree of accuracy whether the $\text{PWL}_{1,2,1}$ system will have either a small or large amplitude limit cycle for each value of λ, and consequently one can compute an approximate value for λ_c. In the linear regime $\mathcal{R}_1$, the left end-point of L_1 is $(\hat{v}_0, \hat{w}_0) = (0, 0)$ and hence the initial condition is given by $(v_0, w_0) = (\hat{v}_0, w_0) = (0, w_0)$. In our simulations we have used the asymptotic approximation $w_0 = -\lambda\,\epsilon$ (for small values of ϵ) computed in Appendix B.4 (see also [2]). This allows to approximate the initial point in the limit cycle trajectory without knowledge of the trajectory in the previous regime. We show below that the choice of other (small) values for w_0 do not qualitatively alter the picture described here.

As we mentioned earlier in the paper, changes in λ do not affect the stability properties of the corresponding virtual fixed-point $(\bar{v}_1, \bar{w}_1)$ but only its location on the linear piece L_1 (or the extension of L_1 beyond the boundaries of $\mathcal{R}_1$) through the reparametrization given by (14). These changes in the location of the fixed-point $(\bar{v}_1, \bar{w}_1)$ cause changes in the integration constants c_1 and c_2 given by (9) (focus case) and (11) (node case). Note that c_1 and c_2 depend on λ only through $(\bar{v}_1, \bar{w}_1)$ or, alternatively, through the initial conditions referred to the virtual fixed point $(v_0 - \bar{v}_1, w_0 - \bar{w}_1)$.

As a result, neither the frequency μ nor the amplitude coefficient r (exponential factor in the solution (10)) change with λ, but rather as λ incresases the spiraling-out trajectory is initially in a larger amplitude "orbit", measured by $D = D(w_0, \lambda)$ given by (24). We illustrate this in Fig. 14-A for the linear piece L_1 (red line) with slope $\eta_1 = 0.3$ and the other parameters used in Figs. 5 and 12 ($\alpha = 4$ and $\epsilon = 0.01$). Trajectories corresponding to increasing values of λ intersect L_1 and reverse

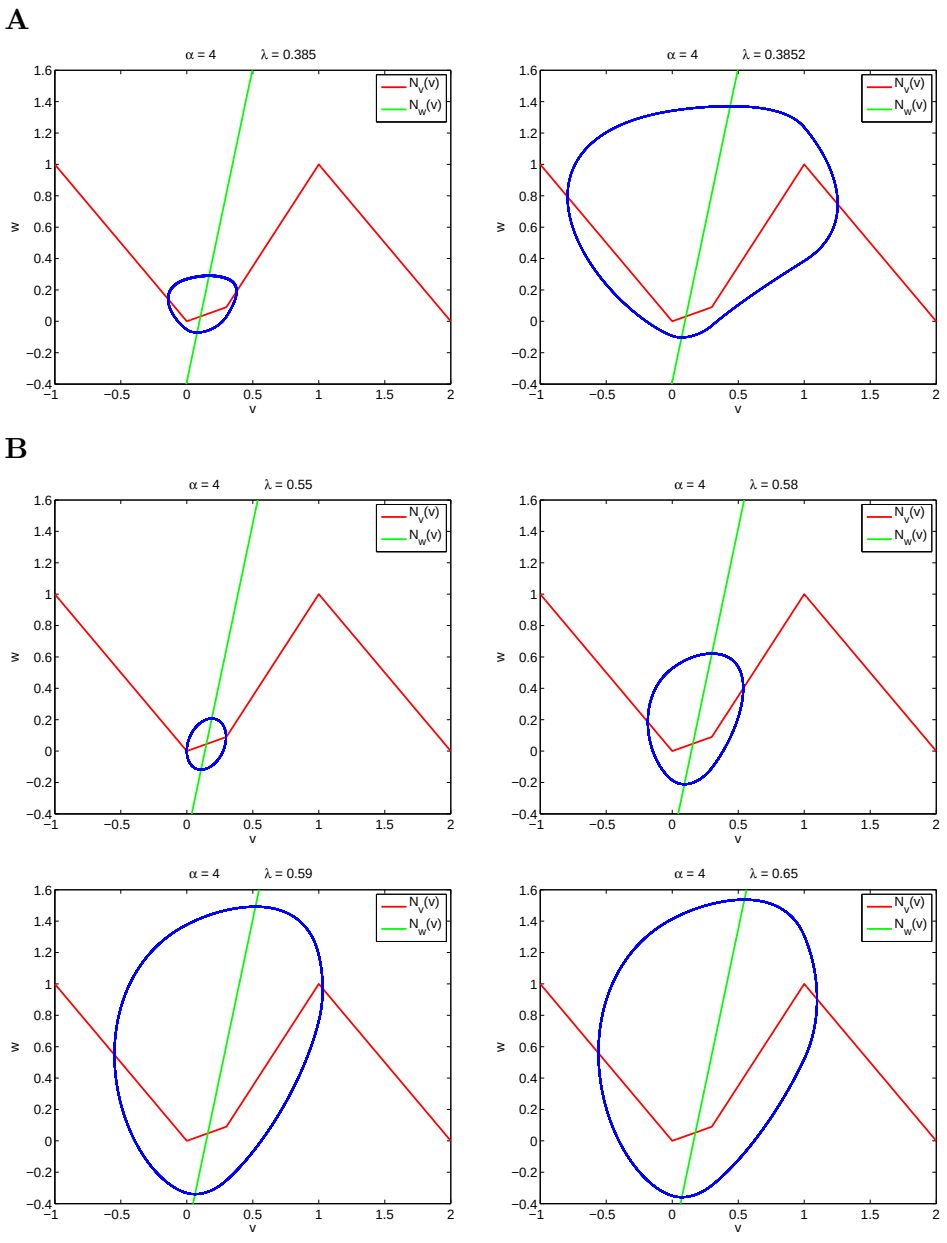

Figure 13: **Transition from small to large amplitude limit cycles in a PWL$_{1,2,1}$ model of FHN type.** We used $v_1 = 0.3$, $\eta_1 = 0.3$, and the parameters presented in Table 1 (sets I and II). **A** $\epsilon = 0.1$. **B** $\epsilon = 0.3$.

their direction at the *reversing*, or *turning*, points (v_{rev}, w_{rev}) whose coordinates increase with λ (the reversing points move to the right). In Fig. 14-B we plot v_{rev} as a function of λ for various values of η and α. The green line in the left panel corresponds to the parameters in Fig. 14-A. This figure shows that the dependence of v_{rev} with λ is linear for all values of η ($< \eta_{cr}^{+}$) and α considered; i.e.,

$$v_{rev} = v(t_{rev}) = \kappa(\eta, \epsilon, \alpha)\ \lambda, \tag{27}$$

and that the slope κ increases with increasing values of η and decreasing values of α.

The curves v_{rev} vs. λ have been calculated using the following formulas derived in Appendix B.2:

$$v_{rev} = v(t_{rev}), \qquad\qquad w_{rev} = w(t_{rev}) \tag{28}$$

with

$$t_{rev} = \frac{1}{\mu} \tan^{-1} \frac{c_2\,\mu + c_1\,r}{c_1\,\mu - c_2\,r}, \tag{29}$$

where c_1, c_2, μ, r are given by (11), (12) and (13), and depend on α, ϵ, η_1 and λ. If for a given parameter set α, ϵ and λ, and η_1 and $\hat{v}_1$ (which determine $|L_1|$) the point $(v_{rev}, w_{rev}) \in L_1$ ($v_{rev} \leq \hat{v}_1$), then the trajectory crosses L_1 and a small amplitude limit cycle is created. If, on the other hand, $v_{rev} > \hat{v}_1$, then the trajectory moves into regime $\mathcal{R}_2$ and, to a first approximation, a large amplitude limit cycle is created.

The values of λ for which a limit cycle trajectory crosses L_1 are bounded by $\lambda < \hat{v}_1/\kappa$ since $v_{rev} < \hat{v}_1$. The larger κ, the smaller the range of values of λ for which trajectories can cross L_1 and create small amplitude limit cycles. Following our previous ideas, we take

$$\lambda_c = \hat{v}_1/\kappa \tag{30}$$

as an approximation to the canard critical value. For the parameters in Fig. 5-B $\lambda_c = 0.029$. This approximation assumes that $\mathcal{R}_2$ does not support small amplitude limit cycles limit cycles; i.e., large amplitude limit cycles are created $v_{rev} > v_1$. As we discussed above, although small amplitude limit cycles trajectories are able to move away from $\mathcal{R}_1$ into $\mathcal{R}_2$ and cross L_2 (Fig. 5-C), this occours for a range of values of λ which is small as compared to λ_c. In the next sections we present appropriate quantitative comparisons.

The linear dependence of v_{rev} with λ given by eq. (27) can be analytically shown to occur in $\mathcal{R}_1$ if in addition to $(\hat{v}, \hat{w}) = (0, 0)$ and $v_0 = 0$ one uses the asymptotic approximation $w_0 = -\lambda\,\epsilon$ (see Appendix B.4). We show in Appendix B.2 that under these conditions eq. (29) becomes

$$t_{rev} = \frac{1}{\mu} \tan^{-1} \frac{-2\,\mu}{2 + \eta - \epsilon} \tag{31}$$

with

$$\kappa(\eta, \epsilon, \alpha) = \frac{2}{\alpha - \eta}\ \frac{-1 - \eta + \epsilon - \epsilon\,\alpha + \epsilon\,\eta}{2 + \eta - \epsilon}\ \cos(\mu\,t_{rev})\ e^{(\eta - \epsilon)\,t_{rev}/2}. \tag{32}$$

Note that the slope κ is independent of λ.

Linear dependence of the turning points v_{rev} with λ is maintained even if we lift the assumption $w_0 = -\lambda\,\epsilon$ although in this case we cannot obtain an analytic expression. We illustrate this in Fig. 15-B for $w_0 = -0.01$ and $w_0 = -0.001$. As w_0 increases in absolute value (the initial point in $\mathcal{R}_1$ is further below the minimum of the v-nullcline), v_{rev} increases thus favoring the transition to $\mathcal{R}_2$. Similar arguments to these presented here can be applied to models having a larger number of linear pieces as we will see in Section 4.

Dependence of λ_c with other model parameters

As Fig 14-B illustrates, the slopes κ increase with η (left panel) and decrease with α (comparison between left and right panels), and so λ_c $(= \hat{v}_1 \,/\, \kappa)$ decrease with η and increase with α. In other words, for fixed values of ϵ, increases in the value of η and decreases in the value of α favor the "escape" from $\mathcal{R}_1$ without crossing the v nullcline, and so the creation of large amplitude limit cycles for smaller value of λ.

The dependence of κ with η is not linear as eq. (32) and Fig. 14-B show. In Fig. 15-A we present the curves $\kappa(\eta)$ for various values of ϵ and two values of α: $\alpha = 4$ (left panel) and $\alpha = 2$ (right panel). The domains of these graphs are bounded by η_{cr}^{+} (7) in order to keep $\mathcal{R}_1$ as an unstable focus regime. The curves $\kappa(\eta)$ are asymptotic to the vertical lines $\eta = \eta_{cr}^{+}$ (not shown). As we can see in Fig. 15-A, κ is a decreasing function of ϵ. From our discussion in the previous paragraphs, λ_c decreases with increasing values of κ, and hence is a decreasing function of η and an increasing function of both α and ϵ, consistent with the canard critical value for smooth FHN systems given by eq. (54) in Appendix A.

In Fig. 16-A we show the predicted values of λ_c as a function of η for two values of α ($\alpha = 4$ and $\alpha = 2$) and two values of ϵ ($\epsilon = 0.01$ and $\epsilon = 0.05$).

For certain parameter regimes it is possible for bistable periodic behavior to occur. One example of this is shown in Fig. 6A. In this case an unstable periodic orbit exists that separates large and small orbits. Under parameter variation this unstable medium size orbit is killed in a saddle-node of periodics bifurcation. When it collides with the large orbit this must occur when two orbits, one with $v \geq 1$ and the other with $v \leq 1$, collide. It is thus interesting to track the point in parameter space where an unstable orbit passes through $v = 1$ and is maximal (which means that the orbit passes through the right hand knee of the voltage nullcline). An example is shown in Fig. 17. Likewise we could consider an unstable medium size orbit that collides with a small stable orbit, which amounts to tracking the small stable orbit which passes through $(v, w) = (\hat{v}, \hat{w})$ as shown in the inset of Fig. 17. Similar constructions have also been explored in [38]. However, to delineate canard transitions it is useful to consider tracking orbits which pass through points of inflection on sections where $v = \hat{v}$. Curves of this type are also plotted in Fig. 17 and we see that the combination of these curves defines a tongue of small but finite width, emanating from $(\lambda, \epsilon) \sim (0, \epsilon_c)$, that separates small from large amplitude oscillations. Here ϵ_c is the critical value above which the inflection line exists, and can be determined as a condition on the eigenvalues $r_{1,2}$ in equation (5) to be real (see also Appendix B.5). This gives $\epsilon_c = 2\alpha - \eta_2 - 2\sqrt{\alpha(\alpha - \eta_2)}$. Interestingly large amplitude unstable periodic solutions on the branch that tracks those which pass through a point of inflection can have a shape exhibiting that of a so-called maximal canard. An example of such an orbit is shown in Fig. 17 (inset bottom right)

A

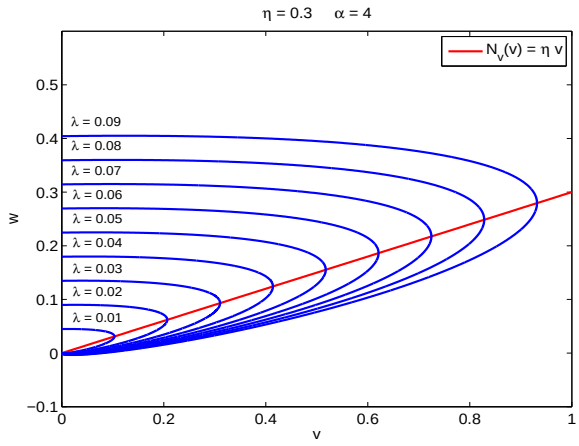

B

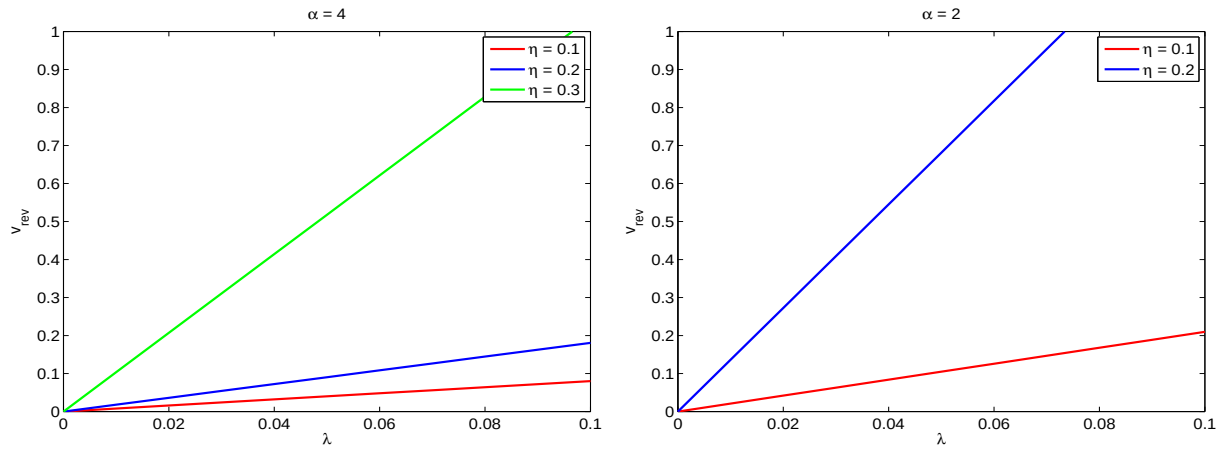

Figure 14: **A** Nine Spiraling out trajectories different amplitudes. They correspond, from smaller to larger amplitude, to $\lambda = 0.01, 0.02, 0.03, 0.04, 0.05, 0.06, 0.07, 0.08, 0.09$. Each trajectory starts at $(v, w) \sim (0, -\lambda\,\epsilon)$ and intersects the linear piece of the v-nullcline $N_v(v)$ at points called (v_{rev}, w_{rev}). Parameters: $\alpha = 4$, $\eta = 0.3$, $r = (\eta - \epsilon)/2 = 0.145$, $\mu = 0.126$. **B** Curves of v_{rev} as a function of λ for various values of η. **Left panel:** $\alpha = 4$ and $\epsilon = 0.01$. **Right panel:** $\alpha = 2$ and $\epsilon = 0.01$. Note that the v-coordinate of the fixed point is $\bar{v} = \lambda/(\alpha - \eta)$.

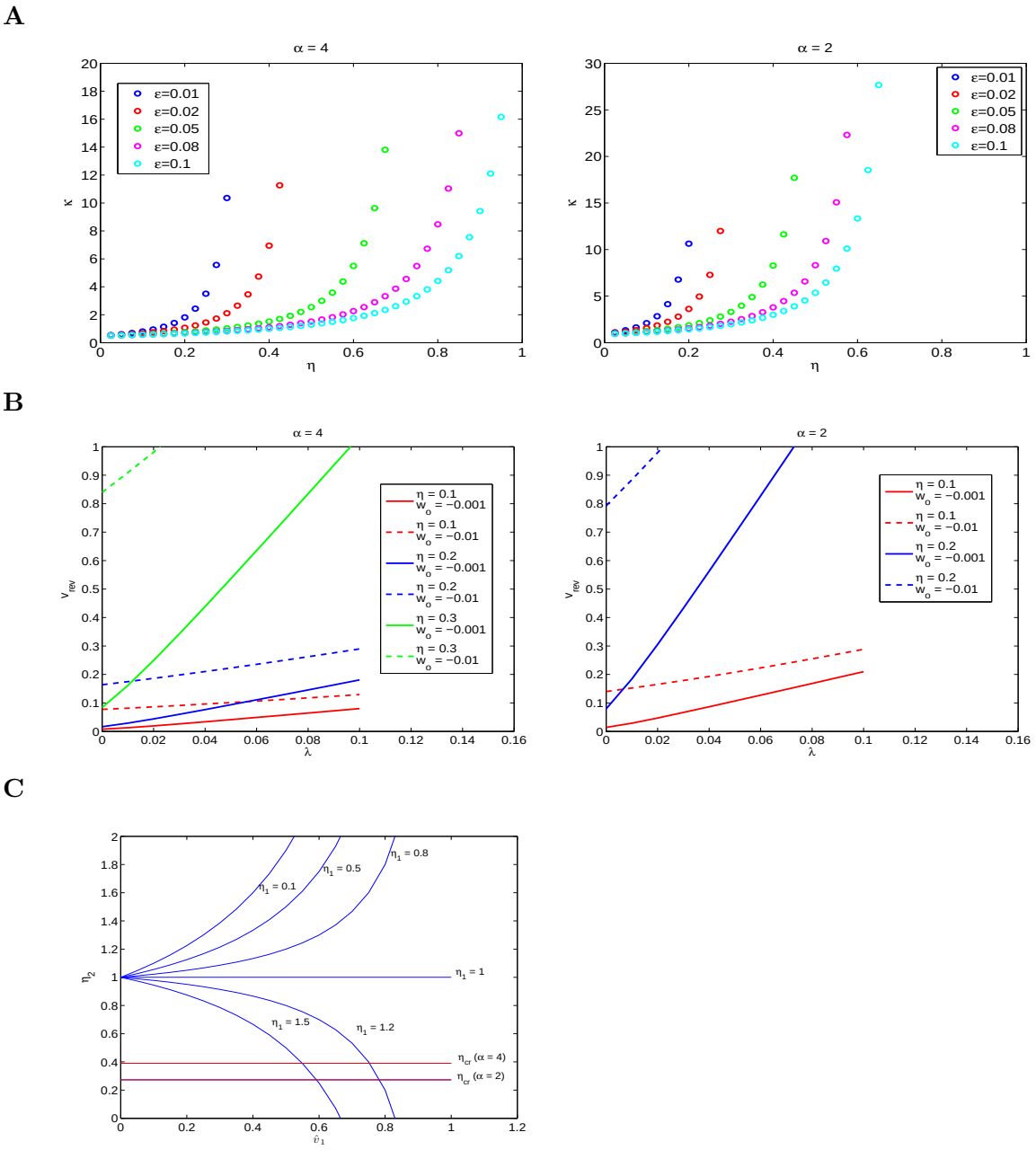

Figure 15: **A** Slope $\kappa(\eta, \epsilon, \alpha)$ of the turning point lines in (27) as a function of η (slope of the linear piece) for various values of α and ϵ. **B** Reversing (or turning) points v_{rev} as a function of λ for various values of η and α, and various initial points $(0, w_0)$ in $\mathcal{R}_1$. **C** Slope η_2 of the linear piece L_2 as a function of v-coordinate v_1 of the joint point between the linear pieces L_1 and L_2 for various values of the slope η_1 of the linear piece L_1 and α.

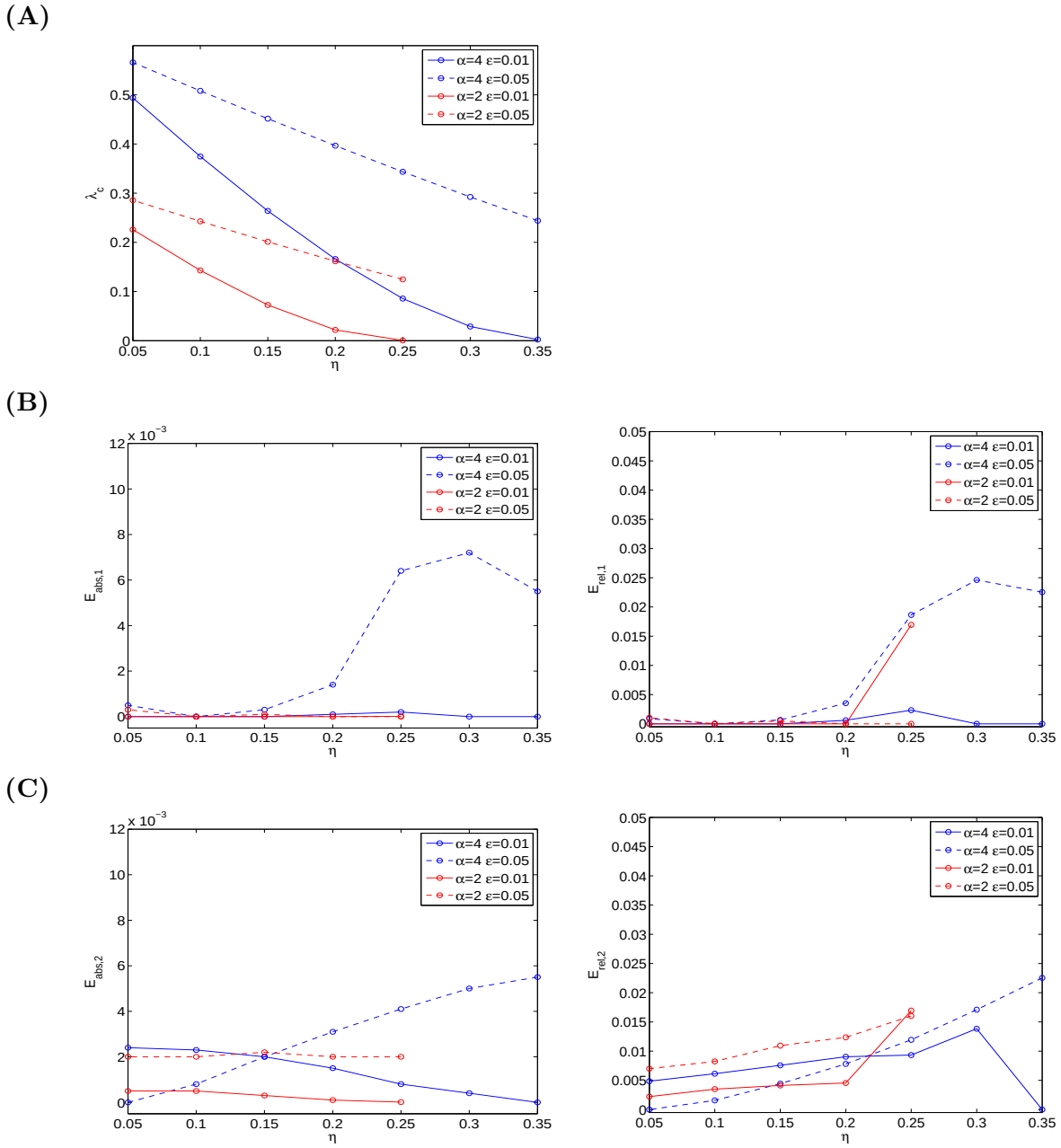

Figure 16: **(A)** Analytical values of λ_c as a function of η for various values of α and ϵ. **(B)** Absolute and relative error between λ_c and the corresponding numerical approximations to the maximum values of λ for which the limit cycle trajectory does not cross from $\mathcal{R}_1$ to $\mathcal{R}_2$. **(C)** Absolute and relative error between λ_c and the corresponding numerical approximations to the maximum values of λ for which the limit cycle trajectory crosses from $\mathcal{R}_1$ to $\mathcal{R}_2$ but still is a small amplitude limit cycle.

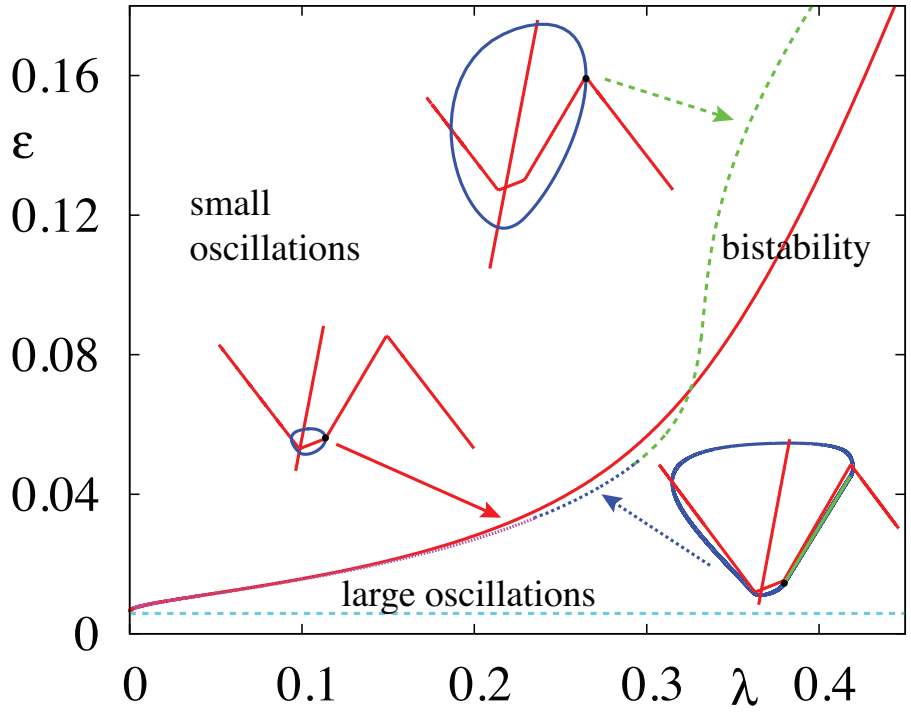

Figure 17: Two parameter bifurcation of the PWL system for Fig. 7. For $(\lambda, \epsilon) \sim (0, \epsilon_c)$ we see a tongue structure that separates large from small amplitude oscillations. The canard point resides within this narrow tongue. For small λ the upper curve is defined by a small amplitude orbit passing through the point $(\hat{v}, \hat{w})$ shown as a filled black circle in the inset. This line separates small amplitude from medium amplitude orbits. The lower curve tracks orbits that pass through a point of inflection on the section $v = \hat{v}$. With increasing λ these orbits increase in size and the branch of solutions ultimately connects with the branch of large amplitude periodic orbits that pass through the right hand knee of the voltage nullcline. These unstable orbits can have shapes like those of maximal canards. For larger values of λ (~ 0.32) bistability of periodic solutions can occur. The horizontal line shows the value of ϵ_c, above which lines of inflection can exist (a necessary condition for canard solutions to exist).

where we also plot the line of inflection (in solid green). The maximal canard trajectory follows the inflection line for part of its trajectory and passes close to the right hand knee of the voltage nullcline. Smaller amplitude orbits that pass through an inflection point occur for smaller values of λ, and this branch of solutions is very close to that defining the border between small stable and medium unstable orbits.

Accuracy of the analytical approximation

In order to check the accuracy of the analytical predictions $\lambda_c = \hat{v}_1 \,/\, \kappa$ described above we compare them with the numerical approximations to both the maximum value of λ for which the limit cycle trajectory does not cross from $\mathcal{R}_1$ to $\mathcal{R}_2$ and the maximum value of λ for which the limit cycle trajectory crosses from $\mathcal{R}_1$ to $\mathcal{R}_2$ but still is a small amplitude limit cycle. We call these approximations $\tilde{\lambda}_{c,1}$ and $\tilde{\lambda}_{c,2}$ respectively. We define the absolute and relative errors as follows

$$E_{abs,1} = |\, \lambda_c - \tilde{\lambda}_{c,1} \,|, \qquad E_{abs,2} = |\, \lambda_c - \tilde{\lambda}_{c,2} \,|, \tag{33}$$

and

$$E_{rel,1} = \frac{E_{abs,1}}{\lambda_c}, \qquad E_{rel,2} = \frac{E_{abs,2}}{\lambda_c}. \tag{34}$$

Our results are presented in Figs. 16-B and -C. The analytical prediction $\lambda_c = \hat{v}_1 \,/\, \kappa$ described above provides a good approximation to the more accurate, numerically calculated, canard critical value $\lambda_{c,2}$.

3.6 No small amplitude limit cycles exist when $\mathcal{R}_1$ is an unstable node regime

No small amplitude limit cycles exist in $\mathcal{R}_1$ when it is an unstable node regime

In contrast to the situation described above, if the linear piece L_1 has slope $\eta_1 > \eta_{cr}$, then the fixed point $(\bar{v}_1, \bar{w}_1)$ (both virtual and actual) is an unstable node. In this case, due to the time scale separation, trajectories arriving to $\mathcal{R}_1$ move almost horizontally, along a fast direction, and no small amplitude limit cycles are generated; i.e., the PWL system displays relaxation (large amplitude) oscillations for all values of λ. As in the focus case, in order for the trajectories to display small amplitude oscillations, they should be able to intersect the linear piece L_1 of the v-nullcline. We show in Appendix B.3 that for nodes these intersection points can be calculated using eqs. (28) and

$$t_{rev} = \frac{1}{r_1 - r_2} \ \ln \frac{-c_2\, r_2}{c_1\, r_1}, \tag{35}$$

where r_1, r_2, c_1 and c_2 are given by (6) and (9). Since $r_1 - r_2 = \sqrt{(\eta + \epsilon)^2 - 4\,\alpha\,\epsilon} > 0$, in order for t_{rev} to be positive (a necessary condiction for the trajectory to intersect L_1) the following condition has to be satisfied:

$$Q = -\frac{c_2\, r_2}{c_1\, r_1} = \frac{(v_0 - \bar{v})\ (r_2 + \epsilon) - (w_0 - \bar{w})}{(v_0 - \bar{v})\ (r_1 + \epsilon) - (w_0 - \bar{w})}\ \frac{r_2}{r_1} > 1. \tag{36}$$

We now show that $Q < 1$ in $\mathcal{R}_1$ for all values of λ; i.e., the trajectory never intersects the linear piece L_1 if the virtual fixed-point in $\mathcal{R}_1$ is a node.

The left-endpoint for L_1 has coordinates $\hat{v} = \hat{w} = 0$ and the initial condition in $\mathcal{R}_1$ has $v_0 = 0$. From eq. 5, the fixed-point (both virtual and actual) is given by $\bar{v} = \lambda/(\alpha - \eta)$ and $\bar{w} = \lambda\eta/(\alpha - \eta)$. Substituting these values in (36), using eq. (6) and the facts that $r_{1,2} + \epsilon - \eta = -r_{2,1}$ and $r_1 r_2 = \epsilon\, \alpha$, and rearranging terms we get

$$Q(\lambda) = \frac{\lambda - q_2}{\lambda - q_1} \tag{37}$$

with

$$q_1 = \frac{w_0\ (\alpha - \eta)\ r_1}{\alpha\, \epsilon} \qquad \text{and} \qquad q_2 = \frac{w_0\ (\alpha - \eta)\ r_2}{\alpha\, \epsilon}. \tag{38}$$

Clearly, $Q(0) = r_2/r_1 < 1$. If there exist a value of $\lambda > 0$ such that $Q(\lambda) = 1$, then $r_2 = r_1$ which can only occur if $\eta = \eta_{cr}$ but $\eta > \eta_{cr}$. Alternatively, if there exist a $\lambda > 0$ such that $Q(\lambda) > 1$, then $r_1 < r_2$ since $w_0 < 0$, but $r_1 > r_2 > 0$. Note that our argument relies on the fact that $w_0 < \hat{w} = 0$. This is always true in $\mathcal{R}_1$ but not in other regimes as we will see in Section 4 when we investigate a $\text{PWL}_{1,3,1}$ system. Note also that, since $dQ/d\lambda = w_0\,(\alpha - \eta)\,(r_2 - r_1)\,/\,(\alpha\,\epsilon)$ and $r_2 - r_1 = -\sqrt{(\eta + \epsilon)^2 - 4\alpha\epsilon} < 0$, then Q is an increasing function of λ for $w_0 < 0$.

No small amplitude limit cycles exist in $\mathcal{R}_2$ when $\mathcal{R}_1$ is an unstable node regime

If $\mathcal{R}_1$ has an unstable node, then $\mathcal{R}_2$ is an unstable focus regime. The slopes η_1 and η_2 of $\mathcal{R}_1$ and $\mathcal{R}_2$ respectively are related by eq. (15) where $0 < \hat{v}_1 < 1$. (If $\hat{v}_1 = 0$, $\hat{v}_1 = 1$ or $\eta_1 = \eta_2 = 1$, then the PWL system has only one linear piece in the middle branch; i.e., it is a $\text{PWL}_{1,1,1}$ system, not a $\text{PWL}_{1,2,1}$ one.) The assumption in Section 3.1 that $0 < \eta_1 < \alpha$ imposes the following constraint on η_2:

$$\eta_2 > \frac{1 - \alpha\, \hat{v}_1}{1 - \hat{v}_1}. \tag{39}$$

Standard algebra shows that $\eta_2 = 1$ for $\hat{v}_1 = 0$, and η_2 is an increasing (decreasing) function of $\hat{v}_1$ for $\eta_1 < 1$ ($\eta_1 > 1$). We show representative curves of η_2 as a function of $\hat{v}_1$ according to eq. (15) in Fig. 15-C. We also show the horizontal lines η_{cr} for $\alpha = 4$ and $\alpha = 2$, and $\epsilon = 0.01$.

A necessary condition for $\mathcal{R}_2$ to have a focus is $\eta_2 < \eta_{cr}$; i.e., η_2 has to be below the line η_{cr} (red line) for some value of $\hat{v}_1$ which together with η_1 determines the length of the linear piece L_1. For the parameters in Figs. 6 ($\alpha = 4$ and $\epsilon = 0.01$), $\eta_{cr} = 0.39$. As discussed in Section 3.1 if $\mathcal{R}_1$ has a focus ($\eta_1 < \eta_{cr} = 0.39$), then $\mathcal{R}_2$ has a node since η_2 is an increasing function of $\hat{v}_1$ for $\eta_1 < 1$. For $\mathcal{R}_2$ to have a focus, L_1 has to be steeper than the line that joins the minimum and maximum of the cubic PWL function ($\eta_1 > 1$) but not as steep so as the endpoint of L_1 is not higher than the maximum of the PWL function. Alternatively, η_{cr} has to increase.

When L_1 is a node and L_2 is a focus only large amplitude limit cycles are created. As we explained earlier, the trajectory arriving at $\mathcal{R}_1$ cannot cross the linear piece L_1 and will move along the fast (horizontal direction) arriving at $\mathcal{R}_2$ with a value of w not very far from its initial value in $\mathcal{R}_1$ ($w_0 < 0$). Since $\eta_2 < \eta_{cr}$, from eq. (15)

$$\hat{w}_1 = \eta_1 \, \hat{v}_1 > 1 - \eta_{cr} \, (1 - \hat{v}_1). \tag{40}$$

That means that initially, the trajectory is not close enough to the point $(\hat{v}_1, \hat{w}_1)$ (left endpoint of the linear piece L_2 so to be able to cross L_2).

4 The canard phenomenon in a $\mathrm{PWL}_{1,3,1}$ models of FHN-type

Here we extend the ideas discussed in Section 3 to PWL systems having three linear pieces in the middle branch of the cubic-like function. More specifically, we consider PWL systems of FHN type described by (2) where $f_{pwl}(v)$ is $\mathrm{PWL}_{1,3,1}$; i.e., it has three linear pieces (L_1, L_2 and L_3) in its middle branch as illustrated in Fig. 18-A. The left and right branches of the graph of $f_{pwl}(v)$ have a single linear piece each, $L_{l,1}$ and $L_{r,1}$ respectively. The values of the slopes (η_1, η_2, η_3, $\eta_{l,1}$ and $\eta_{r,1}$) are presented in Table 2. The dynamics of this system is divided into five linear regimes corresponding to the five linear pieces of $f_{pwl}(v)$ and indexed accordingly. The dynamics of the linear system within each regime is governed by a linear component system of the form (4). The eigenvalues for each linear regime are presented in Table 2. The dynamics on the regimes $\mathcal{R}_{l,1}$ $\mathcal{R}_{r,1}$ (left and right branches) are as in the $\mathrm{PWL}_{1,2,1}$ models discussed in Section 3 (comparison between set I in Tables 1 and Table 2).

In Figs. 18-B, the limit cycle trajectory crosses the linear piece L_1 at its right end-point. Figs. 18-C and -D illustrate the canard phenomenon as λ changes between 0.432 and 0.433. (Table 2, set II). The endpoints $(\hat{v}_1, \hat{w}_1)$ and $(\hat{v}_2, \hat{w}_2)$ joining L_1 to L_2 and L_2 to L_3 respectively were choosen so that the intervals $[0, \hat{v}_1]$, $[\hat{v}_1, \hat{v}_2]$ and $[\hat{v}_2, 1]$ have equal size. The virtual fixed-point $(\bar{v}_1, \bar{w}_1)$ is an unstable focus while the virtual fixed-points $(\bar{v}_2, \bar{w}_2)$ and $(\bar{v}_3, \bar{w}_3)$ are unstable nodes.

The dynamics in $\mathcal{R}_1$ is qualitatively similar to the dynamics in the analogous regime in the $\mathrm{PWL}_{1,2,1}$ models discussed in Section 3 since the virtual fixed-point $(\bar{v}_1, \bar{w}_1)$ is an unstable focus. For values of λ such that the trajectory is able to cross the linear piece L_1 the system has a small amplitude limit cycle whose amplitude increases with λ. In Fig. 18, this occurs for $\lambda \in (0, 0.412)$. For larger values of λ, the trajectory moves into regime $\mathcal{R}_2$ without crossing the linear piece L_1. As for $\mathrm{PWL}_{1,2,1}$ systems, the range of values of λ for which this occurs is very small.

In Fig. 19-A we present graphs of the turning curves v_{rev} versus λ for the parameters in Fig. 18 and three different values of $\eta > \eta_{cr} = 0.39$. The red curves $\eta = 0.6$ correspond to Fig. 18 (since $\eta_2 = 0.6$). The initial values of the trajectory in $\mathcal{R}_2$ are $(\hat{v}_1, w_{2,0}) = (0.33, 0.0166)$ (top panel) and $(\hat{v}_1, w_{2,0}) = (0.33, 0.01)$ (bottom panel). The values of v_{rev} increase, first slowly and then abruptly; small changes in λ cause large increases in v_{rev} marking the fact that the corresponding vector field not longer allows the trajectory to cross the v-nullcline and moves to the right towards the following

	$(\hat{v}, \hat{w})$	η	r_1	r_2	r	μ		set
$L_{l,1}$	$(0, 0)$	-1.0	-0.052	-0.958			S - N	I
$L_{r,1}$		-1.0	-0.052	-0.958			S - N	I
L_1	$(0.33, 0.033)$	0.1			0.192	0.045	U - F	II
L_2	$(0.66, 0.231)$	0.6	0.525	0.065			U - N	II
L_3	$(1, 1)$	2.262	2.244	0.008			U - N	II
L_1	$(0.33, 0.033)$	0.1			0.192	0.045	U - F	III
L_2	$(0.66, 0.132)$	0.3			0.126	0.145	U - F	III
L_3	$(1, 1)$	2.553	2.537	0.006			U - N	III
L_1	$(0.33, 0.033)$	0.1			0.192	0.045	U - F	IV
L_2	$(0.66, 0.693)$	2.0	1.980	0.010			U - N	IV
L_3	$(1, 1)$	0.903	0.857	0.036			U - N	IV

Table 2: $\mathrm{PWL}_{1,3,1}$ models of FHN type for $\alpha = 4$, $\epsilon = 0.01$. The parameters correspond to three models (sets I/II, I/III and I/IV) with the same left and right branches with a single linear piece each (set I). For each linear piece L_j, the table shows the right endpoints $(\hat{v}, \hat{w})$, the slope η, the eigenvalues of the corresponding linear regime (real eigenvalues r_1 and r_2 or real and imaginary parts, $r = (\eta - \epsilon)/2$ and μ respectively if the eigenvalues are complex). The transition from unstable foci (U-F) to unstable nodes (U-N) occurs at $\eta_{cr}^{+} = 0.39$. The transition from stable foci (S-F) to stable nodes (S-N) occurs at $\eta_{cr}^{-} = -0.41$.

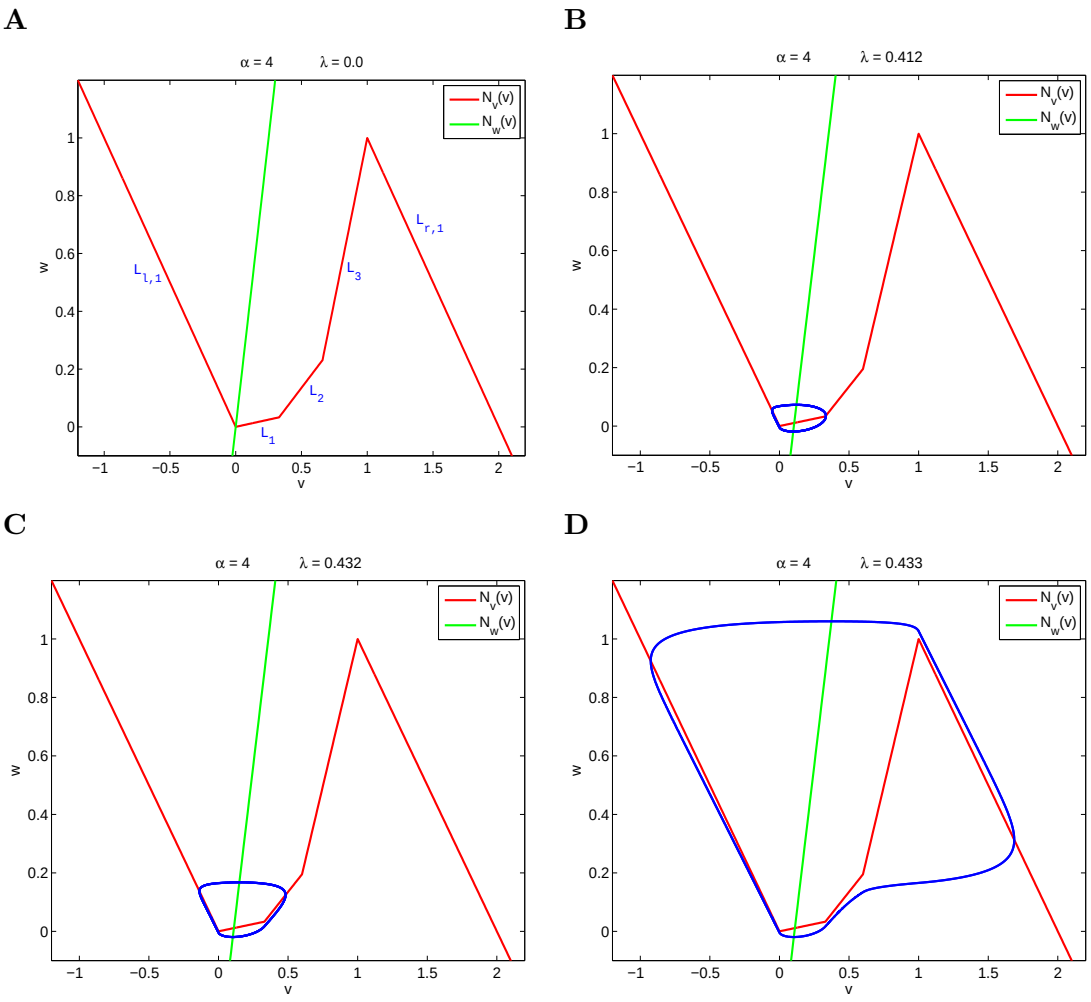

Figure 18: **Canard explosion in a PWL$_{1,3,1}$ system for $\alpha = 4$ and $\epsilon = 0.01$.** **A** Nullclines for $\lambda = 0$. **B** Small amplitude limit cycle where the trajectory crosses L_1 almost at its joint point with the linear piece L_2. **C** Small amplitude limit cycle where the trajectory crosses L_2. **D** Large amplitude limit cycle. The canard explosion occurs for values of $\lambda \in (0.432, 0.433)$. The canard critical value λ_c can be well approximated by the value of λ corresponding to **C**. The corresponding parameters are given in Table 2 (sets I and II).

regime ($\mathcal{R}_3$). This is in contrast to what happens in the "focus" case where the turning curves depend linearly with λ. The range of values of λ for which the trajectory is able to cross the v-nullcline decreases with increasing values of η; i.e., the larger the slope of the linear piece L_2 the shorter the range of intervals of λ for which the intersection between the v-nullcline and the trajectory are possible. As the initial value of the trajectory in $\mathcal{R}_2$ decreases, the turning point curves move to the left (see bottom panel.); i.e., the trajectory's ability to cross the linear piece L_2 decreases. As $w_{2,0}$ decrease further the turning curves "disappear" to the left and trajectories can no longer cross the linear piece L_2.

In Fig. 19-B we present similar curves for $\alpha = 2$ and $w_{2,0} = 0.0166$ (top panel) and $w_{2,0} = 0.0136$ (bottom panel). The behavior is similar to $\alpha = 4$. By comparing the top panels of Fig. 19-B we observe that as α decreases the ability of trajectories to cross the linear piece L_2 also decreases. The value of $w_{2,0}$ used in the bottom panel in Fig. 19-B is larger than that used in Fig. 19-A.

Two additional representative examples are shown in Fig. 20. The corresponding parameters are presented in Table 2 (sets III and IV). These are the same as in Fig. 18 with the exception of η_2 and η_3 that has to satisfy the following constraint

$$\eta_3 = \frac{1 - \eta_2\, \hat{v}_2}{1 - \hat{v}_2}. \tag{41}$$

In Fig. 20-A η_2 is smaller than in Figs. 18 and $\mathcal{R}_2$ has an unstable focus rather than an unstable node. Similarly to the behavior in $\mathcal{R}_1$, the canard explosion occurs when the $v_{rev} > \hat{v}_2$ and the trajectory is able to move to $\mathcal{R}_3$. In Fig. 20-B $\eta_2 = 2$ is larger than in Fig. 18-B ($\eta_2 = 0.6$) and $\mathcal{R}_2$ has an unstable node as in Fig. 18. However, differentely from Fig. 18, this value of η_2 is too large for the turning curves to exist so the trajectory is not able to cross the linear piece L_2 and moves to $\mathcal{R}_3$.

5 Discussion

Classical (smooth) models of FitzHugh-Nagumo (FHN) type (1) are prototypical caricature models of excitable and oscillatory systems in a variety of fields including neuroscience, chemistry and biology [8, 9, 10, 11]. When there exists a time-scale separation between the two participating variables ($\epsilon \ll 1$), these models exhibit abrupt transitions between small and large amplitude oscillations (SAOs and LAOs), known as canard explosions, as a control parameter (λ) moves across a very small critical range [1, 2, 3, 4, 5, 6, 7]. In the context of neural models SAOs and LAOs correspond to subthreshold membrane potential oscillations and action potentials respectively [39, 40, 41, 42].

In this paper, we have investigated the dynamics of two-dimensional, piecewise linear (PWL) models of FHN type (2). $\text{PWL}_{1,1,1}$ models of FHN type (Figs. 3-A and -B, top-left panels) display oscillations in a single amplitude regime (around the left and right branches of the v-nullcline) and hence they do not support canard-like transitions that require two amplitude modes of operation. Canard-like transitions have been shown to occur, numerically, in $\text{PWL}_{1,2,1}$ models of FHN type [33]. In this paper, using geometric and dynamic tools, we have provided a mechanistic explanation of the dynamics of these models including the canard-like explosion of limit cycles, we have shown that the

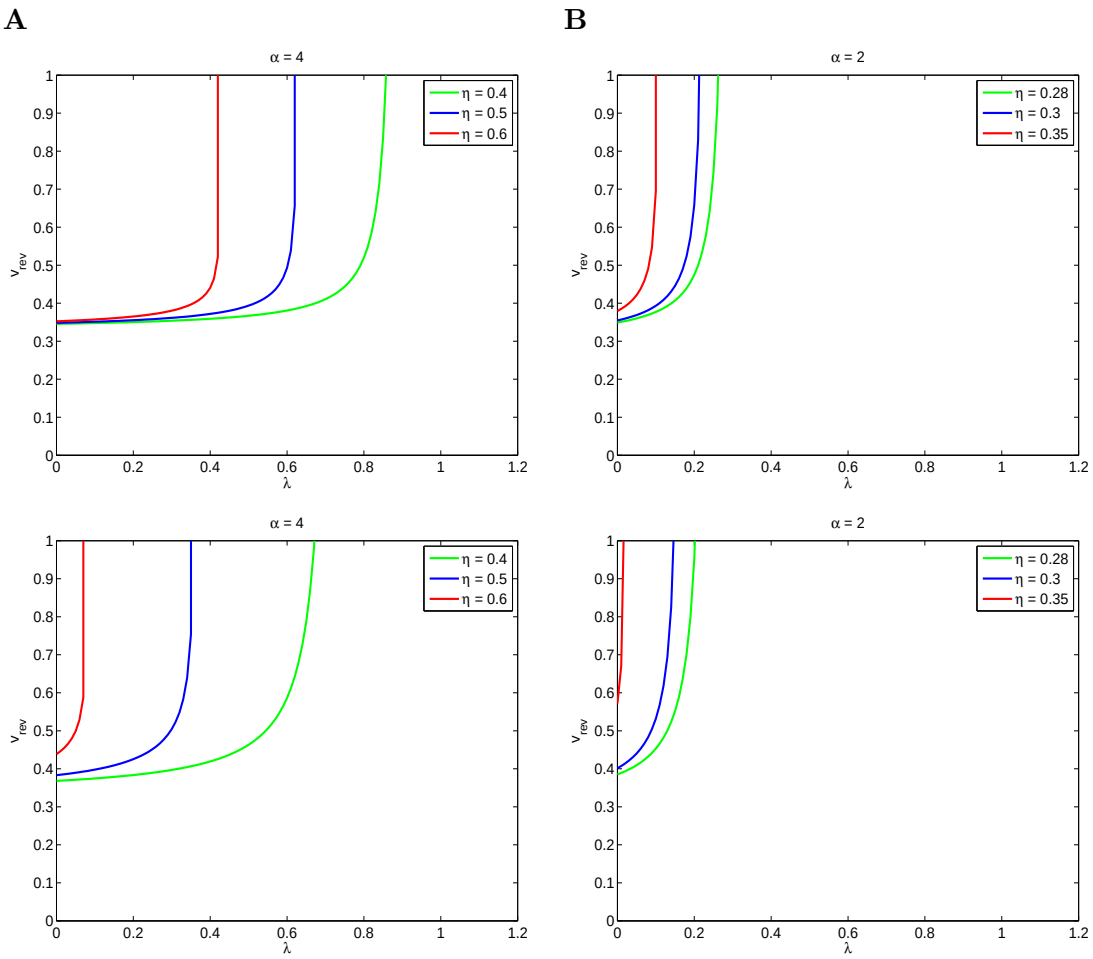

Figure 19: **Reversing (or turning) points v_{rev} in L_2 as a function of λ for various values of α, η and initial points (v_0, w_0) in L_2.** The parameters we used are: $(\hat{v}, \hat{w}) = (0.33, 0.033)$, $v_0 = \hat{v}$, $\epsilon = 0.01$, **A** $\alpha = 4$, $\eta_{cr} = 0.39$, $\eta = 0.4$ ($r_1 = 0.240$ and $r_2 = 0.140$) $\eta = 0.5$ ($r_1 = 0.040$ and $r_2 = 0.087$) $\eta = 0.6$ ($r_1 = 0.053$ and $r_2 = 0.065$) $w_0 = 0.0166$ (top panel), $w_0 = 0.01$ (bottom panel). **B** $\alpha = 2$, $\eta_{cr} = 0.273$, $\eta = 0.28$ ($r_1 = 0.167$ and $r_2 = 0.103$) $\eta = 0.3$ ($r_1 = 0.208$ and $r_2 = 0.082$) $\eta = 0.35$ ($r_1 = 0.281$ and $r_2 = 0.059$) $w_0 = 0.0166$ (top panel), $w_0 = 0.0136$ (bottom panel).

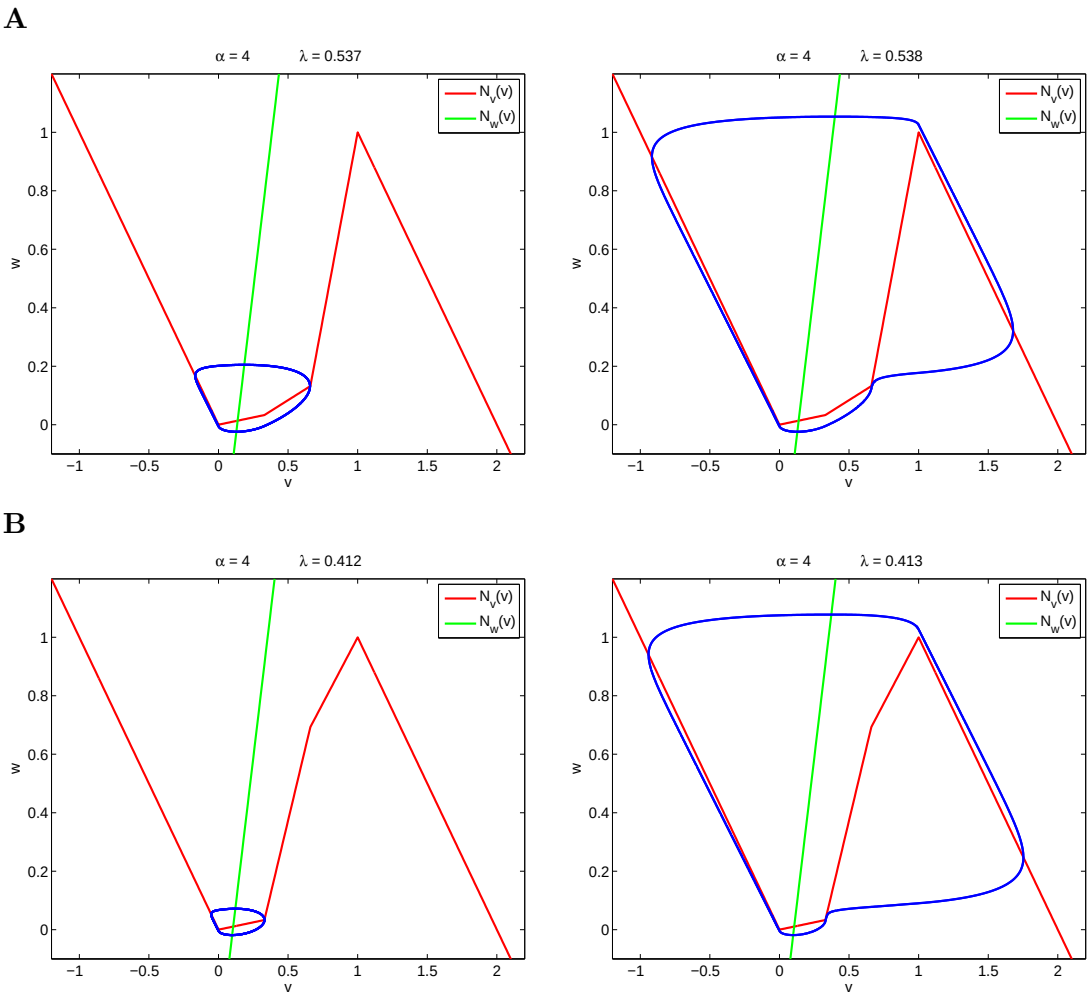

Figure 20: **Canard explosion in a $\mathbf{PWL}_{1,3,1}$ system for $\alpha = 4$ and various piecewise linear configurations in the middle branch of the v-nullcline.** The corresponding parameters are given in **A-B:** Table 2, set III and **C-D:** Table 2, set IV.

mechanistic principles extracted from this study can be extended to $\text{PWL}_{1,3,1}$ models, and we argue that they can be further extended to the investigation of PWL models with a larger number of linear pieces. In addition, the tools we develop and discuss in this paper are amenable for the investigation of a variety of related, and more complex, problems including forced, stochastic and coupled oscillators of FHN type [42, 43, 44, 45, 38].

For a $\text{PWL}_{1,2,1}$ model, a small amplitude limit cycle is created provided the limit cycle trajectory is able to cross the middle branch of the v-nullcline which consists of the linear pieces L_1 and L_2. Otherwise, a large amplitude limit cycle is created. If the linear regime $\mathcal{R}_1$ (corresponding to L_1) has an unstable node, then no small amplitude limit cycles exist; due to the difference in time-scales between the participating variables, the limit cycle trajectory moves fast along an almost horizontal direction and crosses the stable branch of the v-nullcline but never its middle branch. On the other hand, if the linear regime $\mathcal{R}_1$ has an unstable focus, then the limit cycle trajectory is able to cross the linear piece L_1 and generate a small amplitude oscillation provided L_1 is long enough for this intersection to occur within $\mathcal{R}_1$. This picture is analogous to the dynamics generated in smooth cubic-like systems undergoing a sub-critical and super-critical Hopf bifurcations respectively.

For a given size of the linear piece L_1, we showed that the maximum value of the control parameter λ for which the limit cycle trajectory crosses L_1 can be approximated analytically from the model parameters. In addition, we showed that this value of λ gives a good approximation to the numerically computed canard critical value λ_c, and its dependence on the model parameters is consistent with the canard critical value computed by other authors for smooth systems [2, 6]. Limit cycle trajectories moving to the linear regime $\mathcal{R}_2$ can still cross the linear piece L_2 and generate small amplitude limit cycles for slightly larger values of λ but that range of values of λ for which this occurs is very small (order of magnitude of ϵ).

The calculations mentioned above require knowledge of the initial conditions of the limit cycle trajectory in $\mathcal{R}_1$ which in turn would require knowledge of this trajectory in the previous regimes eventually going back to $\mathcal{R}_1$. However, time-scale separation allows for the estimation of these initial conditions in $\mathcal{R}_1$ using asymptotic techniques thus making this estimation independent of the information from previous regimes. Note, however, that for larger values of ϵ the time-scale separation dilutes and this approximation becomes less accurate.

The considerations in the previous paragraph provide a heuristic algorithmic rule for deciding to a good degree of accuracy whether a given set of parameters will give rise to either SAOs or LAOs. Given the initial conditions of the limit cycle trajectory in $\mathcal{R}_1$, the slope η_1 of the linear piece L_1, and the v-coordinate $\hat{v}_1$ of the joint point between the linear pieces L_1 and L_2:

- If $\mathcal{R}_1$ has an unstable node, then the system displays LAOs.
- If $\mathcal{R}_1$ has an unstable focus , then compute the v-coordinate $v_{rev,1}$ of the intersection point between the limit cycle trajectory and the linear piece L_1.
  - If $v_{rev,1} \leq \hat{v}_1$, then the system displays SAOs.
  - If $v_{rev,1} > \hat{v}_1$, then the system displays LAOs.

The last step in this algorithm is based on the fact that if $\mathcal{R}_1$ has a focus, then $\mathcal{R}_2$ has a node. The frequency of the LAOs can be calculated following standard procedures for relaxation oscillators (see

[9]) for example.). The frequency of SAOs is given by the reciprocal of the sum of the times the small amplitude limit cycle trajectory spends moving in a vicinity of the left branch of the v-nullcline and on $\mathcal{R}_1$ (the transition from the latter to the former regimes is very fast). The frequency component corresponding to the latter is given by μ in (12) with η substituted by η_1.

The previous algorithm can be extended to $\text{PWL}_{1,3,1}$ systems. Given the initial conditions of the limit cycle trajectory in $\mathcal{R}_1$, the slopes η_1 and η_2, and the v-coordinates $\hat{v}_1$ and $\hat{v}_2$ (v-coordinates of the joint points between the linear pieces L_1 & L_2 and L_2 & L_3 respectively):

- If $\mathcal{R}_1$ has a node (unstable), then the system displays LAOs.
- If $\mathcal{R}_1$ has a focus (unstable), then compute the v-coordinate $v_{rev,1}$ of the intersection point between the limit cycle trajectory and the linear piece L_1.
  - If $v_{rev,1} \leq \hat{v}_1$, then the system displays SAOs.
  - If $v_{rev,1} > \hat{v}_1$, then (the trajectory moves to $\mathcal{R}_2$)
    - if $\mathcal{R}_2$ has a node (unstable), then the system displays LAOs.
    - if $\mathcal{R}_2$ has a focus (unstable), then **(1)** compute the w coordinate of the trajectory at $\hat{v}_1$ (see Appendix B) and use it as initial condition for the trajectory in $\mathcal{R}_2$, and **(2)** compute the v-coordinate $v_{rev,2}$ of the intersection point between the limit cycle trajectory and the linear piece L_2.
      - if $v_{rev,2} \leq \hat{v}_2$, then the system displays SAOs.
      - if $v_{rev,2} > \hat{v}_2$, then the system displays LAOs.

Althouth we do not provide a rigourous argument on the accuracy of this algorithm, specially as the values of ϵ increase and the time scale separation dilutes, it illustrates the dynamics of the limit cycle trajectory in the vicinity of the unstable branch of the v-nullcline, and it helps in establishing an organizing principle to understanding the dynamics of systems with a larger number of linear pieces. As long as the limit cycle trajectory is in a "focus-regime", it evolves by spiraling out around the virtual fixed-point of the corresponding linear piece. It can either cross the v-nullcline, thus generating a small amplitude limit cycle, or move to the next regime. Only when the trajectory arrives to a "node-regime", it escapes towards the right branch of the v-nullcline thus generating a large amplitude limit cycle. The "last" value of λ for which the trajectory is able to cross a linear piece corresponding to a "focus-regime" provides a good approximation to the canard critical value. We conjecture that this is still true for systems with a larger number of linear pieces in the middle branch. Note that a larger number of linear pieces in either of the other two branches (left and right) has almost no effect on the dynamics of the system in the middle-branch regimes provided there is a well defined time-scale separation between the two participating variables. The frequency profile of the SAOs includes the frequencies μ corresponding to all the "foci-regimes" the trajectory visits, possibly weighted by the size of the corresponding linear piece (or any other measure characterizing the linear regimes).

A salient feature of the dynamics of fast-slow systems exhibiting the canard phenomenon is that trajectories evolve in close vicinities of the unstable (middle) branch of the v-nullcline for a significant

amount of time before creating either SAOs or LAOs, as we illustrate in Fig. 1-A (middle and bottom panels) for a prototypical smooth system of FHN type. Smooth cubic-like functions can be "piecewise-linearized" following the procedure described in Section 2.2. For the example in Fig. 1-A, the PWL middle branch consists of a sequence of linear pieces whose slopes first increase and then decrease (see Fig. 3). From left to right, they correspond to a "focus-", "node-" and again "focus-" regimes respectively. Following our reasoning in the previous paragraphs, trajectories stay close to the unstable branches of the v-nullclines for a significant amount of time because they are spiraling out around the virtual fixed-points corresponding to the regimes they are subsequently visiting.

The previous arguments can be carried to the limit as the size of the linear pieces goes to zero as we illustrate in Fig. 3. In this case, linear pieces are substituted by the tangent line to the cubic-like function at each of its points.

Previous work on canard explosion of limit cycles has assumed time-scale separation between the two participating variables ($\epsilon \ll 1$) [1, 2, 3, 4, 5, 6, 7]. Our results and tools are applicable to systems with a more diluted time-scale separation with values of ϵ intermediate between these and $\mathcal{O}(1)$. In addition, they are applicable to the investigation of the dynamics of forced and coupled oscillators including sub- and super-threshold resonance problems and the construction of phase or spike-time response curves and spike-time difference maps to investigate the synchronization properties of coupled oscillators. In these cases typical perturbation terms are sinusoidal, pulsatile or synaptic-like with various different rise- and decay-times. Limit cycle trajectories evolving in vicinities of the stable branches of the v-nullcline may not feel the effect to these perturbations since they rapidly relax to their original trajectory. However, trajectories evolving in the middle branch may feel significant effects. For instance, a forcing term on the first equation in $\mathrm{PWL}_{1,2,1}$ system will cause a displacement of the v-nullcline with respect to the w-nullcline. This in turn causes changes dynamic displacement of the virtual fixed-point, and in the function (24). As a result, orbits corresponding to SAOs in the unperturbed regime may transiently become LAOs and vice-versa causing the advance or delay of spikes by a significant amount of time with respect to the unperturbed oscillation.

References

[1] F. Dumortier and R. Roussarie. Canard cycles and center manifolds. *Memoirs of the American Mathematical Society*, 121 (577):1–100, 1996.

[2] W. Eckhaus. Relaxation oscillations including a standard chase on French ducks. *In Lecture Notes in Mathematics, Springer-Verlag*, 985:449–497, 1983.

[3] S. M. Baer and T. Erneux. Singular Hopf bifurcation to relaxation oscillations. *SIAM J. Appl. Math.*, 52:1651–1664, 1992.

[4] E. Benoit, J. L. Callot, F Diener, and Diener M. *Chasse au Canard*, volume 31. Collect. Math., 1981.

[5] M. Krupa and P. Szmolyan. Relaxation oscillation and canard explosion. *J. Diff. Eq.*, 174:312–368, 2001.

[6] M. Krupa and P. Szmolyan. Extending geometric singular perturbation theory to nonhyperbolic points - fold and canard points in two dimensions. *SIAM J. Math. Anal.*, 33(2):286–314, 2001.

[7] F. Dumortier. Techniques in the theory of local bifurcations: Blow-up, normal forms, nilpotent bifurcations, singular perturbations. *In Bifurcations and Periodic Orbits of Vector Fields, edited by D. Schlomiuk (Kluwer Academic Press, Dordrecht)*, pages 19–73, 1993.

[8] J. D. Murray. *Mathematical Biology.* Springer, Berlin, 1989.

[9] S. H. Strogatz. *Nonlinear Dynamics and Chaos.* Addison Wesley, Reading MA, 1994.

[10] R. FitzHugh. Impulses and physiological states in models of nerve membrane. *Biophys. J.*, 1:445–466, 1961.

[11] F. C. Hoppensteadt. *An Introduction to the Mathematics of Neurons.* Cambridge Univ. Press, NY, 1996.

[12] H. P. McKean. Nagumo's equation. *Advances in Mathematics*, 4:209–223, 1970.

[13] R. Fitzhugh. Impulses and physiological states in theoretical models of nerve membranes. *Biophysical Journal*, 1182:445–466, 1961.

[14] W. P. Wang. Multiple impulse solutions to McKean's caricature of the nerve equation. I. Existence. *Communications on pure and applied mathematics*, 41:71–103, 1988.

[15] W. P. Wang. Multiple impulse solutions to McKean's caricature of the nerve equation. II. Stability. *Communications on pure and applied mathematics*, 41:997–1025, 1988.

[16] A. Tonnelier. The McKean's caricature of the FitzHugh-Nagumo model I. The space-clamped system. *SIAM Journal on Applied Mathematics*, 63:459–484, 2002.

[17] J. Rinzel and J. B. Keller. Traveling wave solutions of a nerve conduction equation. *Biophysical J.*, 13:1313–1337, 1973.

[18] J. Rinzel. Neutrally stable traveling wave solutions of nerve conduction equations. *J. Math. Biol.*, 2:205–217, 1975.

[19] J. Rinzel. Spatial stability of traveling wave solutions of a nerve conduction equation. *Biophysical J.*, 15:975–988, 1975.

[20] S. Coombes and A. H. Osbaldestin. Period adding bifurcations and chaos in a periodically stimulated excitable neural relaxation oscillator. *Physical Review E*, 62:4057–4066, 2000.

[21] A. Tonnelier and W. Gerstner. Piecewise linear differential equations and integrate-and-fire neurons: Insights from two-dimensional membrane models. *Physical Review E*, 67:021908(1–16), 2003.

[22] S. Coombes. Neuronal networks with gap junctions: A study of piece-wise linear planar neuron models. *SIAM Journal on Applied Dynamical Systems*, 7:1101–1129, 2008.

[23] S. J. Hogan. On the dynamics of rigid-block motion under harmonic forcing. *Proceedings of the Royal Society of London. Series A*, 425:441–476, 1989.

[24] S. H. Doole and S. J. Hogan. Non-linear dynamics of the extended Lazer-McKenna bridge oscillation model. *Dynamics and Stability of Systems*, 15:43–58, 2000.

[25] M. di Bernardo, C. Budd, A. R. Champneys, and P. Kowalczyk. *Piecewise-smooth Dynamical Systems: Theory and Applications*. Springer, 2007.

[26] G. M. Maggio, M. di Bernardo, and M. P. Kennedy. Nonsmooth bifurcations in a piecewise-linear model of the Colpitts oscillator. *IEEE Transactions on Circuts and Systems-I: Fundamental Theory and Applications*, 47:1160–1177, 2000.

[27] A. F. Filippov. *Differential Equations with Discontinuous Righthand Sides*. Kluwer Academic Publishers, Dordrecht, 1988.

[28] E. Plahte and S. Kjoglum. Analysis and generic properties of gene regulatory networks with graded response functions. *Physica D*, 201:150–176, 2005.

[29] F. Grognard, H. de Jong, and J.-L. Gouzé. *Biology and Control Theory : Current Challenges*, chapter Piecewise-linear models of genetic regulatory networks : Theory and example, pages 137–159. Lecture Notes in Control and Information Science (LNCIS) 357. Springer, 2007.

[30] J. Llibre, E. Nu nez, and A. E. Teruel. Limit cycles for planar piecewise linear differential systems via first integrals. *Qualitative theory of dynamical systems*, 3:29–50, 2002.

[31] E. Freire, E. Ponce, F. Rodrigo, and F. Torres. Bifurcation sets of continuous piecewise linear systems with two zones. *International Journal of Bifurcation and Chaos*, 8:2073–2097, 1998.

[32] E. Freire, E. Ponce, and J. Ros. Limit cycle bifurcations from center in symmetric piecewise-linear systems. *International Journal of Bifurcation and Chaos*, 9:895–907, 1999.

[33] N. Arima, H. Okazaki, and H. Nakano. A generation mechanism of canards in a piecewise linear system. *IEICE Transactions on Fundamentals of Electronics, Communications and Computer Sciences*, E80:447–453, 1997.

[34] W. E. Boyce and R. C. DiPrima. *Elementary differential equations and boundary value problems*. John Wiley and Sons, Hoboken, NJ, 2009.

[35] B. Peng, V. Gaspar, and K. Showalter. False bifurcations in chemical systems: Canards. *Philosophical Transactions of the Royal Society of London. Series A*, 337:275–289, 1991.

[36] M. Brons and K. Bar-Eli. Asymptotic analysis of canards in the EOE equations and the role of the inflection line. *Proceedings of the Royal Society of London. Series A*, 445:305–322, 1994.

[37] M. Desroches and M. R. Jeffrey. Canard à l'orange: a new recipe for studying relaxation oscillations. *preprint*, 2010.

[38] D. J. W. Simpson and R. Kuske. Mixed-mode oscillations in a stochastic piecewise-linear system. *Physica D*, 240:1189–1198, 2011.

[39] C. T. Dickson, J. Magistretti, M. H Shalinsky, E. Fransén, M. Hasselmo, and A. A. Alonso. Properties and role of I_h in the pacing of subthreshold oscillation in entorhinal cortex layer II neurons. *J. Neurophysiol.*, 83:2562–2579, 2000.

[40] H. G. Rotstein, T. Oppermann, J. A. White, and N. Kopell. A reduced model for medial entorhinal cortex stellate cells: Subthreshold oscillations, spiking and synchronization. *Journal of Computational Neuroscience*, 21:271–292, 2006.

[41] H. G. Rotstein, M. Wechselberger, and N. Kopell. Canard induced mixed-mode oscillations in a medial entorhinal cortex layer II stellate cell model. *SIAM J. Appl. Dyn. Sys.*, 7:1582–1611, 2008.

[42] V. A. Makarov, V. I. Nekorkin, and M. G. Velarde. Spiking behavior in a noise-driven system combining oscillatory and excitatory properties. *Phys. Rev. Lett.*, 15:3031–3034, 2001.

[43] H. G. Rotstein, N. Kopell, A. Zhabotinsky, and I. R. Epstein. A canard mechanism for localization in systems of globally coupled oscillators. *SIAM J. Appl. Math.*, 63:1998–2019, 2003.

[44] H. G. Rotstein and R. Kuske. Localized and asynchronous patterns via canards in coupled calcium oscillators. *Physica D*, 215:46–61, 2006.

[45] M. A. Zaks, X. Sailer, L. Schimansky-Geier, and A. B. Neiman. Noise induced complexity: From subthreshold oscillations to spiking in coupled systems. *Chaos*, 15:026117, 2005.

[46] H. G. Rotstein, D. Pervouchine, M. J. Gillies, C. D. Acker, J. A. White, E. H. Buhl, M. A. Whittington, and N. Kopell. Slow and fast inhibition and h-current interact to create a theta rhythm in a model of CA1 interneuron networks. *J. Neurophysiol.*, 94:1509–1518, 2005.

Acknowledgments

This work was partially supported by the National Science Foundation grant DMS-0817241 (HGR). SC would like to acknowledge discussions with Kyle Wedgwood regarding canards in PWL systems.

A Hopf bifurcation and canard critical values for two-dimensional relaxation oscillators

The general form of a two-dimensional relaxation oscillator is given by

$$\begin{cases} v' = F(v,w), \\ w' = \epsilon\, G(v,w;\lambda). \end{cases} \tag{42}$$

System (42) is fast-slow for $\epsilon \ll 1$. The zero level curves $F(v,w) = 0$ and $G(v,w) = 0$ define the nullclines of system (42). We assume that the curve $F(v,w) = 0$ can be expressed as $w = f(v)$ with $f(v)$ a cubic-like function having one local minimum at (v_m, w_m) and one local maximum at (v_M, w_M) with $v_m < v_M$ and $w_m < w_M$. In the example shown in Fig. 1, $f(v) = -2\,v^3 + 3\,v^2$, $(v_m, w_m) = (0,0)$ and $(v_M, w_M) = (1,1)$. Without loss of generality, in the following discussion we take $(v_m, w_m) = (0,0)$. The function $G(v,w;\lambda)$ is assumed to be a non-increasing function of w such that the zero level curve $G(v,w;\lambda) = 0$ is an increasing function of v for every λ in a given neighborhood of $\lambda = 0$, and is also a decreasing function of λ for all v in a neighborhood of v_m. In the

example shown in Fig. 1, $G(v, w; \lambda)$ is expressed as $w = g(v; \lambda) = \alpha\, v - \lambda$. We further assume that $F(v, w) = 0$ and $G(v, w; \lambda)$ intersect at $(\bar{v}, \bar{w}) = (v_m, w_m)$ when $\lambda = 0$ and $\bar{v} > v_m$ ($\bar{v} < v_m$) when $\lambda > 0$ ($\lambda < 0$). The FitzHugh-Nagumo (FHN) and van der Pol (VDP) systems discussed below in Sections A.3 and A.4 are particular cases of system (42).

A.1 Hopf bifurcation

For $\lambda = 0$, the nullclines of system (42) are assumed to intersect at the minimum of the cubic-like nullcline $F(v, w) = 0$; i.e., $(\bar{v}, \bar{w}) = (v_m, w_m)$. A Hopf bifurcation occurs when λ crosses the Hopf bifuraction point $\lambda_H > 0$ given by ([5, 46])

$$\lambda_H(\sqrt{\epsilon}) = -\frac{G_w}{2\,(G_v)^{1/2}\,|F_w|^{1/2}}\epsilon + \mathcal{O}(\epsilon^{3/2}), \tag{43}$$

where all the functions are calculated at $(v_{min}, w_{min}, \lambda = 0)$. For values of $\lambda < \lambda_H$, fixed points $(\bar{v}, \bar{w})$ are stable. At the Hopf bifurcation the fixed point $(\bar{v}, \bar{w})$ becomes unstable and a small amplitude limit cycle is created. This limit cycle is stable or unstable according to the Hopf bifurcation being supercritical or subcritical respectively. The type of criticality of the Hopf bifurcation can be determined by looking at the sign of the criticality parameter Δ which depends on the parameters of the model and is given by [5, 46]

$$\Delta = \frac{2}{|F_w|^{1/2}\,(G_v)^{1/2}\,(F_{vv})^2}\;\Omega \tag{44}$$

with

$$\Omega = G_v\,F_{vv}\,F_{vw} + |F_w|\,G_v\,F_{vvv} - |F_w|\,G_{vv}\,F_{vv} - G_w\,(F_{vv})^2, \tag{45}$$

where all the functions are calculated at $(v_{min}, w_{min}, \lambda = 0)$. The Hopf bifurcation is supercritical if $\Delta < 0$ ($\Omega < 0$) and subcritical if $\Delta > 0$ ($\Omega > 0$). If the Hopf bifurcation is subcritical ($\Delta > 0$), trajectories starting inside the unstable limit cycle converge to the stable fixed point $(\bar{v}, \bar{w})$. On the other hand, if the Hopf bifurcation is supercritical ($\Delta < 0$), trajectories starting inside the limit cycle are attracted to it.

A.2 The canard phenomenon and the canard critical value

Here we follow Krupa and Szmolyan [5, 6]. As mentioned above, the canard explosion occurs in a range of values of λ which is exponentially small in ϵ. For the purpose of our discussion we will refer to this range as λ_c. The following approximation to the canard critical value λ_c has been calculated as a function of the parameters of the model [5, 6, 43]

$$\lambda_c(\sqrt{\epsilon}) = -\frac{G_v}{2\,F_{vv}^3\,|G_\lambda|}[\,G_v\,F_{vw}\,F_{vv} + G_v\,|F_w|\,F_{vvv} - |F_w|\,G_{vv}\,F_{vv} + G_w\,F_{vv}^2\,]\;\epsilon + \mathcal{O}(\epsilon^{3/2}), \tag{46}$$

where all the functions are calculated at the point (v_{min}, w_{min}) and $\lambda = 0$ or, more generally, for the value of λ corresponding to the intersection between the two nullclines ocurring at the minimum of the cubic-like one. Eq. (46) has been calculated under the following assumptions [6] that define a canard (fold) point and will be referred to as the *canard conditions*. They ensure that the nullcline $G(v, w, \lambda) = 0$ (w-nullcline) is transverse to the nullcline $F(v, w) = 0$ (v-nullcline), and it passes through the fold point with non-zero speed as λ varies. Without loss of generality, we take $(v_m, w_m) = (0, 0)$. **(1)** $F(0, 0) = 0$, $\partial F/\partial v(0, 0)) = 0$, $\partial^2 F/\partial v^2(0, 0) \neq 0$, i.e., $(0, 0)$ is a nondegenerate local minimum (fold point) of the nullcline $F(v, w) = 0$ for λ in a suitable interval. **(2)** $\partial F/\partial w(0, 0) \neq 0$. **(3)** $G(0, 0, 0) = 0$, $\partial G/\partial v(0, 0, 0) \neq 0$ and $\partial G/\partial \lambda(0, 0, 0) \neq 0$. The Van der Pol and FitzHugh-Nagumo models discussed below satisfy these conditions.

A.3 Van der Pol type models

Van der Pol (VDP) type models have the following general form

$$\begin{cases} v' = f(v) - w, \\ w' = \epsilon\, [v - \lambda], \end{cases} \tag{47}$$

where $f(v)$ is cubic-like. Here we assume, without lost of generality, that $(v_{min}, w_{min}) = (0, 0)$. The w-nullcline is a vertical line intersecting the v-axis at $v = \lambda$. The fixed point is given by $(\bar{v}, \bar{w}) = (\lambda, f(\lambda))$. From eqs. (43), (44), (45) and (46), the Hopf bifurcation point, the Hopf bifurcation criticality parameter, and the canard critical value are given respectively by

$$\lambda_H = \mathcal{O}(\epsilon^{3/2}) \sim 0 \;\; (> 0), \qquad \Delta = \frac{1}{2\,(f'')^2} f''', \qquad \lambda_c = -\frac{1}{2\,(f'')^3} f'''. \tag{48}$$

If $f(v) = -h\, v^3 + a\, v^2$, then

$$\Delta = -\frac{3\,h}{a^2} < 0, \qquad \lambda_c = \frac{3\,h}{8\,a^3}. \tag{49}$$

Note that for VDP type oscillators the Hopf bifurcation (and the canard phenomenon) is always supercritical.

A.4 FitzHugh-Nagumo type models

FitzHugh-Nagumo type models have the following general form

$$\begin{cases} v' = f(v) - w, \\ w' = \epsilon\, [\, g(v; \lambda) - w\,], \end{cases} \tag{50}$$

where $f(v)$ is cubic like and $g(v; \lambda)$ is either linear of sigmoid-like. Here we assume, without lost of generality, that $(v_{min}, w_{min}) = (0, 0)$. From eqs. (43), (44), (45) and (46), the Hopf bifurcation point, the Hopf bifurcation criticality parameter, and the canard critical value are given respectively by

$$\lambda_H = \frac{1}{2\,(g')^{1/2}} \epsilon + \mathcal{O}(\epsilon^{3/2}), \qquad \Delta = \frac{2}{(g')^{1/2}\,(f'')^2} [\,(f'')^2 + g'\, f''' - g''\, f''\,], \tag{51}$$

and

$$\lambda_c = \frac{g'}{2\,(f'')^3\,|g_\lambda|}\;[(f'')^2 - g'\,f''' + g''\,f'']\;\epsilon + \mathcal{O}(\epsilon^{3/2}). \tag{52}$$

If $f(v) = -h\,v^3 + a\,v^2$, then

$$\Delta = \frac{1}{(g')^{1/2}\,a^2}[\,2\,a^2 - 3\,h\,g' - a\,g''\,], \qquad \lambda_c = \frac{g'}{8\,a^3\,|g_\lambda|}\;[\;2\,a^2 + 3\,h\,g' + a\,g''\,]\;\epsilon + \mathcal{O}(\epsilon^{3/2}). \tag{53}$$

If, in addition, $g(v;\lambda) = \alpha\,v - \lambda$, then

$$\lambda_H = \frac{1}{2\,\alpha^{1/2}}\epsilon + \mathcal{O}(\epsilon^{3/2}), \qquad \Delta = \frac{1}{\alpha^{1/2}\,a^2}\,[\,2\,a^2 - 3\,\alpha\,h\,], \qquad \lambda_c = \frac{\alpha}{8\,a^3}\;[\;2\,a^2 + 3\,\alpha\,h\,]\;\epsilon + \mathcal{O}(\epsilon^{3/2}). \tag{54}$$

Note that the Hopf bifurcation is supercritical (subcritical) if $\alpha > 2a^2/(3h)$ ($\alpha < 2a^2/(3h)$).

B Dynamics of the basic linear components

B.1 Calculation of target values for $(\,\eta + \epsilon\,)^2 - 4\,\epsilon\,\alpha > 0$ (real eigenvalues)

From (8) and (9), the time $\hat{t}$ it takes for the solution $(V, W) = (v - \bar{v}, w - \bar{w})$ to evolve from the initial conditions (V_0, W_0) to the target point (V_T, W_T) is given by

$$\hat{t} = \frac{1}{r_2}\;\ln\frac{(r_2 + \epsilon\,)\,V_T - W_T}{(r_2 + \epsilon\,)\,V_0 - W_0}. \tag{55}$$

Given V_T, W_T must satisfy the following equation:

$$[\,V_0\,(r_1 + \epsilon\,) - W_0\,]\;\left[\frac{V_T\,(r_2 + \epsilon\,) - W_T}{V_0\,(r_2 + \epsilon\,) - W_0}\right]^{\frac{r_1}{r_2}} - [\,V_T\,(r_2 + \epsilon\,) - W_T\,] = V_T\,(r_1 - r_2). \tag{56}$$

Given W_T, V_T must satisfy the following equation:

$$(r_2 + \epsilon\,)\;[\,V_0\,(r_1 + \epsilon\,) - W_0\,]\;\left[\frac{V_T\,(r_2 + \epsilon\,) - W_T}{V_0\,(r_2 + \epsilon\,) - W_0}\right]^{\frac{r_1}{r_2}} -$$

$$-(r_1 + \epsilon\,)\;[\,V_T\,(r_2 + \epsilon\,) - W_T\,] = W_T\,(r_1 - r_2). \tag{57}$$

B.2 Calculation of the intersection point between trajectories and a linear piece of the v-nullcline for $(\eta+\epsilon)^2 - 4\,\epsilon\,\alpha < 0$ (complex eigenvalues)

Here we calculate the intersection points (v_{rev}, w_{rev}) between a trajectory given by eqs. (10) and (11), initially located at (v_0, w_0), and a linear piece in the middle branch of the v-nullcline, described by $w = \eta\,(v - \hat{v}) + \hat{w}$ with $\eta > 0$. We assume that initially the trajectory is below this line; i.e., the trajectory moves to the right and upwards. If the initial points of the trajectory and the linear piece coincide ($v_0 = \hat{v}$) then this implies that $w_0 < \hat{w}$. We use the notation given in (11), (12) and (13).

At the intersection point (v_{rev}, w_{rev}), if it exists, the trajectory reverses direction (changing its direction of motion from left-to-right to right-to-left). The time t_{rev} at which this happens satisfies $dv/dt = 0$ with $dw/dt \neq 0$. By differentiating the first eq. in (10) we get

$$[\,(c_2\,\mu + c_1\,r)\,cos(\mu\,t) + (c_2\,r - c_1\,\mu)\,sin(\mu\,t)\,]\,e^{r\,t} = 0. \tag{58}$$

Thus, t_{rev} is the smallest positive number of the form:

$$t_{rev} = \frac{1}{\mu}\tan^{-1}\frac{c_2\,\mu + c_1\,r}{c_1\,\mu - c_2\,r}, \tag{59}$$

and

$$v_{rev} = v(t_{rev}), \qquad\qquad w_{rev} = w(t_{rev}). \tag{60}$$

Note that if t_{rev} is negative, then a multiple of π should be added to it. Note also that t_{rev}, and so (v_{rev}, w_{rev}), depend on the difference between the initial and fixed points, $(v_0 - \bar{v}, w_0 - \bar{w})$ and not on each of these points separately.

Linear piece L_1

For the linear piece L_1, $\hat{v} = \hat{w} = 0$ and $v_0 = 0$. We further assume $w_0 = -\lambda\,\epsilon$. Then

$$v_0 - \bar{v} = \frac{-\lambda}{\alpha - \eta}, \qquad\qquad w_0 - \bar{w} = \frac{-\lambda\,(\epsilon\,\alpha - \epsilon\,\eta + \eta)}{\alpha - \eta}. \tag{61}$$

Substituting into (9) and rearranging terms yields

$$c_1 = \frac{-\lambda}{\alpha - \eta}, \qquad\qquad c_2\,\mu = \frac{-\lambda}{\alpha - \eta}\;\;\frac{\epsilon - \eta - 2\,\epsilon\,(\alpha - \eta)}{2}. \tag{62}$$

Substituting c_1, c_2, μ and r intro eq. (59) gives a simplified expression for t_{rev}

$$t_{rev} = \frac{1}{\mu}\tan^{-1}\frac{-2\,\mu}{2 + \eta - \epsilon}. \tag{63}$$

From eq. (63),

$$\sin(\mu\;t_{rev}) = -\frac{2\,\mu}{2 + \eta - \epsilon}\;\cos(\mu\;t_{rev}).$$

Substituting into the solution for v in (63) operating algebraically we obtain the following simplified expression:

$$v_{rev} = v(t_{rev}) = \frac{2\,\lambda}{\alpha - \eta} \;\; \frac{-1 - \eta + \epsilon - \epsilon\,\alpha + \epsilon\,\eta}{2 + \eta - \epsilon} \;\; \cos\left(\mu t_{rev}\right) \; e^{(\eta - \epsilon)\, t_{rev}/2}. \tag{64}$$

Clearly, v_{rev} is a linear function of λ with slope

$$\kappa(\eta, \epsilon, \alpha) = \frac{2}{\alpha - \eta} \;\; \frac{-1 - \eta + \epsilon - \epsilon\,\alpha + \epsilon\,\eta}{2 + \eta - \epsilon} \;\; \cos\left(\mu\, t_{rev}\right) \; e^{(\eta - \epsilon)\, t_{rev}/2}. \tag{65}$$

B.3 Calculation of the intersection point between the trajectory and a linear piece of the v-nullcline for $(\,\eta + \epsilon\,\sigma)^2 - 4\,\epsilon\,\alpha > 0$ (real eigenvalues)

Here we calculate the intersection points (v_{rev}, w_{rev}) between a trajectory given by eqs. (8) and (9), initially at (v_0, w_0), and a linear piece in the middle branch of the v-nullcline, described by $w = \eta\,(v - \hat{v}) + \hat{w}$ with $(\eta > 0)$. We assume that initially the trajectory is below this line; i.e., the trajectory moves to the right and upwards. If the initial points of the trajectory and the linear piece coincide $(v_0 = \hat{v})$ then this implies that $w_0 < \hat{w}$. We use the notation

$$r_{1,2} = \frac{\eta - \epsilon\,\sigma \;\pm\; \sqrt{(\eta + \epsilon\,\sigma)^2 - 4\,\epsilon\,\alpha}}{2}, \tag{66}$$

$$c_1 = \frac{(v_0 - \bar{v})\,(r_1 + \epsilon\,\sigma) - (w_0 - \bar{w})}{r_1 - r_2}, \qquad c_2 = \frac{-(v_0 - \bar{v})\,(r_2 + \epsilon\,\sigma) + (w_0 - \bar{w})}{r_1 - r_2}. \tag{67}$$

At the intersection point (v_{rev}, w_{rev}), if it exists, the trajectory reverses direction (changing its direction of motion from left-to-right to right-to-left). The time t_{rev} at which this happens satisfies $dv/dt = 0$ with $dw/dt \neq 0$. By differentiating the first eq. in (8) we get

$$c_1\, r_1\, e^{r_1 t} + c_2\, r_2\, e^{r_2 t} = 0. \tag{68}$$

Thus

$$t_{rev} = \frac{1}{r_1 - r_2} \;\; \ln \frac{-c_2\, r_2}{c_1\, r_1}, \tag{69}$$

and

$$v_{rev} = v(t_{rev}), \qquad\qquad w_{rev} = w(t_{rev}). \tag{70}$$

Note that $r_1 - r_2 = \sqrt{(\eta + \epsilon\,\sigma)^2 - 4\,\alpha\,\epsilon}$.

B.4 Asymptotic behavior of trajectories approximating the limit cycle in the vicinity of the stable branches of the PWL cubic-like nullcline

We consider the FHN type system (1) expressed in terms of the slow variable $\tau = \epsilon\, t$ ($\epsilon \ll 1$).

$$\begin{cases} \epsilon\, \dot{v} = f(v) - w, \\ \dot{w} = \alpha\, v - \lambda - w\ , \end{cases} \tag{71}$$

in a domain where $f'(v) < 0$. In (71) "dot" stands for $d/d\tau$. For $\epsilon = 0$, $w = f(v)$. We follow [2] and investigate the behavior of trajectories in $\mathcal{O}(\epsilon)$ neighborhoods of $w = f(v)$ by introducing the transformation

$$w = f(v) + \epsilon\, \phi. \tag{72}$$

Substitution into (71) yields

$$\frac{\mathrm{d}v}{\mathrm{d}\tau} = -\phi. \tag{73}$$

By differentiating (72) with respect to τ, substituting (73) and using the second equation in (71) we obtain

$$\epsilon\, \frac{\mathrm{d}\phi}{\mathrm{d}\tau} = f'(v)\, \phi + \alpha\, v - \lambda - f(v) - \epsilon\, \phi, \tag{74}$$

or

$$\frac{\mathrm{d}\phi}{\mathrm{d}t} = f'(v)\, \phi + \alpha\, v - \lambda - f(v) - \epsilon\, \phi. \tag{75}$$

The steady state of eq. (74) is given by

$$\bar{\phi} = \frac{f(v) + \lambda - \alpha\, v}{f'(v) - \epsilon}. \tag{76}$$

To a first order approximation in ϵ ($\epsilon \ll 1$) trajectories move fast towards the slow manifold approximated by $w = f(v) + \epsilon\, \bar{\phi}$.

For a linear piece, $f(v) = \eta\, v$ (with $\eta < 0$). Then

$$\bar{\phi}(v) = \frac{(\eta - \alpha)\, v + \lambda}{\eta - \epsilon}, \tag{77}$$

$$\lim_{v \to 0} \bar{\phi}(v) = \frac{\lambda}{\eta - \epsilon} \qquad \text{and} \qquad \lim_{v \to 0} w = \epsilon\, \phi = \epsilon\, \frac{\lambda}{\eta - \epsilon}. \tag{78}$$

B.5 Calculation of the inflection lines

For a general planar system of the form

$$v' = F(v, w), \qquad w' = G(v, w) \tag{79}$$

a point of inflection is defined by

$$\frac{\mathrm{d}}{\mathrm{d}v}\left(\frac{\mathrm{d}w}{\mathrm{d}v}\right) = \frac{F\frac{\mathrm{d}G}{\mathrm{d}v} - G\frac{\mathrm{d}F}{\mathrm{d}v}}{F^2} = 0. \tag{80}$$

Hence, assuming it exists, an inflection point on a trajectory described by $w = w(v)$ is determined by the following geometric condition

$$F\left[\frac{\partial G}{\partial v} + \frac{\partial G}{\partial w}\frac{\mathrm{d}w}{\mathrm{d}v}\right] - G\left[\frac{\partial F}{\partial v} + \frac{\partial F}{\partial w}\frac{\mathrm{d}w}{\mathrm{d}v}\right] = 0. \tag{81}$$

If system (79) is linear with

$$F(v, w) = A_{11}v + A_{12}w + b_1, \qquad G(v, w) = A_{21}v + A_{22}w + b_2, \tag{82}$$

then eq. (81) defines two straight lines of the form $w = w_\pm(v)$, where

$$w_\pm(v) = \frac{v[A_{21}\sigma_\pm - A_{11}] + b_2\sigma_\pm - b_1}{A_{12} - A_{22}\sigma_\pm}, \tag{83}$$

$$\sigma_\pm = \frac{A_{11} - A_{22} \pm \sqrt{(\mathrm{Tr}\, A)^2 - 4\det A}}{2A_{21}}, \tag{84}$$

and

$$A = \begin{pmatrix} A_{11} & A_{12} \\ A_{21} & A_{22} \end{pmatrix}. \tag{85}$$

The *inflection lines* $w_\pm$ only exist if the solutions of (83) are real, which is the case if the matrix A has real eigen-values.
For a linear system of the form (4),

$$A = \begin{bmatrix} \eta_j & -1 \\ \epsilon\alpha & -\epsilon \end{bmatrix} \qquad \text{and} \qquad \begin{bmatrix} b_1 \\ b_2 \end{bmatrix} = \begin{bmatrix} -\eta_j\hat{v}_{j-1} + \hat{w}_{j-1} \\ -\epsilon\lambda \end{bmatrix}. \tag{86}$$

Substituting into (83) and (84) we obtain the inflection line (25). Note that for the singular value $\epsilon = 0$ one of the inflection lines coincides with the voltage nullcline. We define the canard inflection point as the set of parameters for which a periodic orbit develops a point of inflection.

B.6 Proof that the inflection and eigenvector lines coincide

Here we show that the inflection lines (25) and the eigenvector lines (26) coincide. The latter have the eigenvector directions and cross the virtual fixed-point $(\bar{v}_2, \bar{w}_2)$. In the remaining of this section we will drop the subindex from the slope η, the fixed-point $(\bar{v}, \bar{w})$ and the endpoints $(\hat{v}, \hat{w})$. We proceed by showing that both the slopes and the ordinates to the origin coincide; i.e.,

$$\alpha \, \frac{\eta - r_{1,2} - \epsilon}{\alpha - r_{1,2} - \epsilon} = r_{2,1} + \epsilon \tag{87}$$

and

$$\frac{\lambda \, (r_{1,2} + \epsilon) - \alpha \, (\eta \, \hat{v} - \hat{w})}{\alpha - r_{1,2} - \epsilon} = -(r_{2,1} + \epsilon) \, \hat{v} + \hat{w}. \tag{88}$$

First we show that the identity (87) is true. Substituting (6) into (87) gives

$$\alpha \, \frac{2\,\eta - (\eta - \epsilon \pm \sqrt{P}) - 2\,\epsilon}{2\,\alpha - (\eta - \epsilon \pm \sqrt{P}) - 2\,\epsilon} = r_{2,1} + \epsilon \tag{89}$$

where

$$P = (\eta + \epsilon)^2 - 4\,\epsilon\,\alpha \tag{90}$$

Substituting (90) into (89) and rearranging terms gives

$$\alpha \, \frac{\eta - \epsilon \mp \sqrt{P}}{2\,\alpha - \eta - \epsilon \mp \sqrt{P}} = r_{2,1} + \epsilon \tag{91}$$

or

$$\alpha \, \frac{r_{2,1}}{\alpha - \eta + r_{2,1}} = r_{2,1} + \epsilon. \tag{92}$$

Multiplying the denominator in the left hand side of eq. (92) by its right hand side, rearranging terms and using the fact that $r_{2,1}$ are roots of the characteristic polynomial of the matrix A in (86) gives the numerator in the left hand side in eq. (92) showing that the identity (87) is true.

Now we show that the identity (88) is true. We will use the following identity

$$r_{2,1} + \epsilon = \eta - r_{1.2}, \tag{93}$$

that can be calculated using (90), and

$$\eta \, \hat{v} - \hat{w} = \lambda - (\alpha - \eta) \, \bar{v}, \tag{94}$$

that can be calculated from (5). Substituting (93) and (94) into (88) and rearranging terms we obtain

$$(\,\lambda + \bar{w}\,)\,(\,r_{1,2} + \epsilon - \alpha\,) = [\,(r_{1,2} - \eta)\,(\alpha - \epsilon - r_{1,2}) - \alpha\,(\alpha - \eta)\,]\,\bar{v}. \tag{95}$$

Manipulating algebraically the right hand side of eq. (95), using the fact that $r_{2,1}$ are roots of the characteristic polynomial of the matrix A in (86) and rearranging terms we obtain

$$(\lambda + \bar{w}) (r_{1,2} + \epsilon - \alpha) = \alpha (r_{1,2} + \epsilon - \alpha) \bar{v} \tag{96}$$

or

$$(\alpha \bar{v} - \lambda - \bar{w}) (r_{1,2} + \epsilon - \alpha) = 0 \tag{97}$$

which follows from the fact that $(\bar{v}, \bar{w})$ is a fixed-point of the linear system and $w = \alpha v - \lambda$ is its w-nullcline.